NACA
TN
3375
c.1

TECH LIBRARY KAFB, NM
0066461

NACA TN 3375

NATIONAL ADVISORY COMMITTEE FOR AERONAUTICS

TECHNICAL NOTE 3375

A THEORY FOR PREDICTING THE FLOW OF REAL GASES IN SHOCK TUBES WITH EXPERIMENTAL VERIFICATION

By Robert L. Trimpi and Nathaniel B. Cohen

Langley Aeronautical Laboratory
Langley Field, Va.

Washington
March 1955

TECH LIBRARY KAFB, NM
0066461

K

NATIONAL ADVISORY COMMITTEE FOR AERONAUTICS

TECHNICAL NOTE 3375

A THEORY FOR PREDICTING THE FLOW OF REAL GASES IN SHOCK TUBES WITH EXPERIMENTAL VERIFICATION

By Robert L. Trimpi and Nathaniel B. Cohen

SUMMARY

The nonlinear characteristic differential equations applicable to a quasi-one-dimensional unsteady channel flow with friction and heat transfer are linearized and integrated in functional form for the particular study of small perturbations from ideal shock-tube flows. If the equivalence of unsteady- and steady-flow boundary layers is assumed, the problem of determining the perturbations in the unsteady flow reduces to an evaluation of the drag of a flat plate in the equivalent steady flow.

For air at initially uniform temperature, the theory evaluated with an equivalent steady-flow turbulent-boundary-layer skin-friction coefficient predicts that shock attenuation increases with distance and that average values of static pressure, velocity, density, and Mach number at a fixed position in the hot gas increase with time, whereas average sonic speed simultaneously decreases with time at a fixed position.

Experimental measurements of the shock attenuation with distance and static-pressure variation with time at a fixed position for diaphragm pressure ratios from approximately 4 to 18 gave good agreement with the theoretical predictions where a value of $0.0581 \times (\text{Reynolds number})^{-1/5}$ was used for the skin-friction coefficient.

INTRODUCTION

The shock tube has become a common aerodynamic testing facility because of its relative inexpensiveness and versatility. In a shock tube it is possible to obtain unsteady flows with a wide range of flow parameters, such as Reynolds number, Mach number, and temperature, that either could not be obtained in steady-flow apparatus with the present temperature limit of known alloys or could be obtained only with massive and costly equipment.

The various states of the flow of a perfect, nonviscid, nonconducting gas in a shock tube may easily be determined theoretically by application of the basic equations of momentum, continuity, and energy. (See, for example, refs. 1 to 4.) The theoretical states so determined are conical in a distance-time sense (until the shock-tube end effects interfere); that is, parameters are invariant along rays which have the same ratios of distance from the diaphragm station to time elapsed since diaphragm burst. This perfect-gas flow is also characterized by two regions, of equal constant velocity and pressure but of different density and temperature, separated by a contact surface or entropy discontinuity. One of these regions has as its leading boundary the shock wave advancing down the tube into the low-pressure air at rest; whereas the other has as its trailing boundary the expansion wave progressing into the high-pressure section. Therefore, it is theoretically possible to obtain steady-flow aerodynamic data in the short-duration steady flows that exist while either region is passing a fixed point along the shock tube.

Unfortunately, the flow of a real gas in the shock tube departs significantly in many cases from the aforementioned theoretical flow. It is intuitively obvious that a real flow differs from the theoretical flow in that a pressure drop is required of a real fluid flowing in a tube and a further pressure change is required to account for heat transfer between the tube and the fluid. In addition, the flow in the region behind the entropy discontinuity has been found to be quite turbulent and erratic so as to make it of very limited value for most testing purposes. Although the flow between the shock wave and the entropy discontinuity does not degenerate into large-scale turbulence, this flow is still affected by viscosity, heat transfer, other imperfect gas effects, and nonideal diaphragm burst. (See refs. 1, 3, and 4.) The nonideal condition of diaphragm burst may be minimized by the proper choice of diaphragm material for each particular initial set of conditions. However, the other effects are unavoidable, and it is to be expected that their magnitude will increase in importance in the high-temperature and high Mach number range, where the shock tube appears to be otherwise most advantageous.

The attenuation in shock strength as the shock travels down the tube is the most obvious and easily measured deviation from perfect-fluid theory. This attenuation has been the subject of several experimental and theoretical studies (refs. 3, 5, 6, and 7).

The theory of reference 3 may be briefly outlined as follows. The unsteady flow of the hot gas between the shock and entropy discontinuity is reduced to a quasi-steady flow by choosing a coordinate system fixed to the shock. The boundary-layer problem is then reduced to a laminar solution similar to the Blasius solution, except that the wall velocity is nonzero. The unsteady boundary condition of the receding entropy discontinuity is ignored as is the entire cold-flow region between the expansion and entropy discontinuity. The skin-friction and heat-transfer effects obtained from this solution are then averaged across the assumed one-dimensional flow and the resulting changes in average momentum and average energy require the generation of moving waves. These waves are assumed to be generated at the entropy discontinuity and to travel unchanged in strength until they overtake the shock. The shock attenuation is then determined from the waves which have overtaken it since flow was first initiated.

The theories of references 6 and 7 are much less elaborate than that of reference 3 and are based on the assumption that the mass flow through the shock at a certain time is the same as the mass flow at the entropy discontinuity evaluated at the same time. The mass flow at the entropy discontinuity is determined from the boundary-layer displacement thickness and free-stream conditions corresponding to an unattenuated shock. This boundary-layer displacement thickness is determined in references 6 and 7 from an extension, to a circular tube and rectangular tube, respectively, of the Rayleigh problem of the instantaneous acceleration to constant velocity of a flat plate in a fluid at rest.

In an unpublished analysis made at the Langley Aeronautical Laboratory, Messrs. Paul W. Huber, Donald R. McFarland, and Philip Levine collaborated on a theory for shock attenuation based on the mass-flow decrement due to displacement thickness at the entropy discontinuity. In order to determine the shock attenuation at a given time, the displacement thickness was evaluated in this theory for a time smaller than this given time by an interval equal to the wave-travel time from the entropy discontinuity to the shock. This displacement thickness was determined from empirical flat-plate steady-flow data at a distance from the leading edge of the flat plate equal to the distance from the diaphragm station to the entropy discontinuity.

None of the aforementioned theories have given good agreement with experimentally determined shock attenuation. Reference 8 reports the use of a chrono-interferometer to obtain the timewise variation of density in the two theoretically constant density regions. A density rise with time was noted for both regions. Comparison of the experimental data with the theory of reference 3 gave poor correlation. By employing various simplified flow models, the aforementioned theories have ignored the fact that unsteady waves are continually being generated by the effects of friction and heat transfer in the entire flow region. The result of these waves overtaking the shock is attenuation, and their motion along the tube results in variations in pressure, density, and velocity at given points. Therefore, in order to obtain a satisfactory understanding of the flow of a real gas in a shock tube, a theory must recognize and treat the wave system in the entire flow field. Such a theory has been derived in simplified form, and this theory, together with experimental correlation obtained at the Gas Dynamics Branch of the Langley Laboratory, is presented in this paper.

SYMBOLS

A	area of flow
a	velocity of sound
B	constant defined by equation (D4)
c_f	local skin-friction coefficient, $2\tau/\rho U^2$
c_v	coefficient of specific heat at constant volume
c_p	coefficient of specific heat at constant pressure
D	hydraulic diameter, $\frac{4 \times \text{Area}}{\text{Perimeter}}$
$\frac{D(\ )}{Dt}$	convective derivative, $\frac{\partial(\ )}{\partial t} + U \frac{\partial(\ )}{\partial x}$
H_f	heat added per unit mass by frictional dissipation
h	wall heat-transfer coefficient
J	heat added per unit mass due to heat transfer and heat sources
l	fixed distance along shock-tube axis
$M = U/a$	
$M_\alpha = U/a_\alpha$	
$M_\beta = U/a_\beta$	
$M_s = U_s/a_\infty$	
$M_v = V/a_\infty$	
$M_w = W/a_\epsilon$	
N	defined in equation (53)
n	reciprocal of velocity exponent in boundary layer, $\frac{u_y}{U} = \left(\frac{y}{\delta}\right)^{1/n}$

P	characteristic parameter, $\frac{2c_v}{R} a + U$
P'	effective characteristic wave parameter, $P - \frac{a}{\gamma} \frac{S}{R}$
P_r	Prandtl number
p	static pressure
p_{v_s}	static pressure immediately behind shock
Q	characteristic parameter, $\frac{2c_v}{R} a - U$
Q'	effective characteristic wave parameter, $Q - \frac{a}{\gamma} \frac{S}{R}$
R	gas constant
R_e	Reynolds number
r	recovery factor
S	entropy
T	temperature
t	time
U	free-stream velocity
U^*	shearing-stress velocity, $\sqrt{\tau/\rho}$
U_s	shock velocity
u_y	velocity in boundary layer at y
V	velocity of ray in x,t plot of figure 1, x_v/t_v
W	velocity of ray in x,t plot of figure 1, x_w/t_w
x	distance along shock tube from diaphragm station
y	distance from surface

γ	ratio of specific heats, c_p/c_v; assumed = 1.40 for computations
δ	boundary-layer thickness; also indicates differential quantity
$\frac{\delta(\ )}{\delta t}$	characteristic derivative, $\frac{\partial(\ )}{\partial t} + (U \pm a)\frac{\partial(\ )}{\partial x}$
$\eta = \frac{a_\epsilon}{a_\alpha}$	
θ	difference between wall temperature and adiabatic recovery temperature of flow
μ	coefficient of viscosity
ν	coefficient of kinematic viscosity
ξ	distance flow has progressed along surface
ρ	density
$\sigma = \frac{a_\infty}{a_\beta}$	
τ	wall shearing stress
$\phi_{P_\alpha}, \phi_{Q_\alpha}, \phi_{P_\beta}, \phi_{Q_\beta}, \phi_{s_\alpha}, \phi_{s_\beta}$	influence coefficients, defined in equations (12), (13), and (26)

Subscripts:

Subscripts not included on the symbols defined above refer, in general, to values at points or within regions shown in figure 1. Exceptions to be noted, however, are as follows:

o	perfect-fluid value
t	at time t
x	at distance x
exp	experimental
ref	reference value
theor	theoretical

THEORY

The basic steps followed in deriving the theory are first outlined. The characteristic differential equations for a quasi-one-dimensional unsteady channel flow are linearized on the basis of the perfect-fluid flow in a shock tube. The terms of these equations for a particular lamina of fluid in the shock tube are expressed as functions of the distance the lamina has moved along the shock tube. A transformation of variables of integration is then made whereby the time integral of the characteristic equation is replaced by a distance integral along the particle path. The values of the flow variables, such as pressure, velocity, temperature, and so forth, may then be found from the values of the integrated characteristic parameters.

One method of evaluating the resulting integrals is to assume the equivalency of steady and unsteady flows based on particle-flow time. Application of this method reduces the solution for the characteristic equations to the simple computation of the skin-friction integral (total drag) of a flat plate in steady flow.

The characteristic equations for a quasi-one-dimensional unsteady channel flow as derived in appendix A are:

$$\frac{\delta P}{\delta t} = -a\,\frac{D \log_e A}{Dt} + \frac{a}{\gamma}\,\frac{\delta \frac{S}{R}}{\delta t} + \frac{\gamma - 1}{\gamma}\,a\,\frac{D \frac{S}{R}}{Dt} - \frac{2U^2 c_f}{D} \qquad (1)$$

$$\frac{\delta Q}{\delta t} = -a\,\frac{D \log_e A}{Dt} + \frac{a}{\gamma}\,\frac{\delta \frac{S}{R}}{\delta t} + \frac{\gamma - 1}{\gamma}\,a\,\frac{D \frac{S}{R}}{Dt} + \frac{2U^2 c_f}{D} \qquad (2)$$

Furthermore, under the assumption that the relation between skin friction and heat transfer is the same for both steady and unsteady flows, the convective derivative of entropy may be expressed (see appendix B) as

$$\frac{D \frac{S}{R}}{Dt} = \left(M^2 + \frac{1}{\gamma - 1}\,\frac{\theta}{T}\,P_r^{-2/3}\right)\frac{2\gamma}{D}\,Uc_f \qquad (3)$$

For application to the study of flows in a shock tube, the preceding equations are linearized by assuming that all coefficients and differential operators on the right-hand side are constant at their respective perfect-fluid values. In other words, the lines making up the perfect-fluid characteristics network are used as paths of integration, and the various derivatives and coefficients are evaluated on the basis of the velocities, temperatures, and so forth, of the perfect fluid. Equations (1) to (3) then become, if linearized on this basis (subscript o refers to perfect fluid),

$$\frac{\delta P}{\delta t} = -a_o\left(\frac{D \log_e A}{Dt}\right)_o + \frac{a_o}{\gamma}\left(\frac{\delta \frac{S}{R}}{\delta t}\right)_o + \frac{\gamma - 1}{\gamma} a_o\left(\frac{D \frac{S}{R}}{Dt}\right)_o - \frac{2U_o{}^2 c_f}{D} \tag{1a}$$

$$\frac{\delta Q}{\delta t} = -a_o\left(\frac{D \log_e A}{Dt}\right)_o + \frac{a_o}{\gamma}\left(\frac{\delta \frac{S}{R}}{\delta t}\right)_o + \frac{\gamma - 1}{\gamma} a_o\left(\frac{D \frac{S}{R}}{Dt}\right)_o + \frac{2U_o{}^2 c_f}{D} \tag{2a}$$

$$\left(\frac{D \frac{S}{R}}{Dt}\right)_o = \left(M_o{}^2 + \frac{1}{\gamma - 1} \frac{\theta_o}{T_o} P_r{}^{-2/3}\right)\frac{2\gamma}{D} U_o c_f \tag{3a}$$

where

$$\left(\frac{D}{Dt}\right)_o \equiv \frac{\partial}{\partial t} + U_o \frac{\partial}{\partial x}$$

$$\left(\frac{\delta}{\delta t}\right)_o \equiv \left(\frac{D}{Dt}\right)_o \pm a_o \frac{\partial}{\partial x}$$

It is further assumed that, although the velocity of the leading edge of the expansion fan is correctly used as $-a_\epsilon$, the fluid and characteristic velocities may be approximated by U_α and $(U \pm a)_\alpha$ in the entire region from the leading edge of the expansion wave to the entropy discontinuity. This assumption, which greatly simplifies the computations, introduces errors that increase in magnitude as the expansion-fan region increases with shock pressure ratio.

Equations (1a) and (2a) are expressions for the derivatives along characteristics of slope $\frac{\delta x}{\delta t} = (U \pm a)_o$ and equation (3a) evaluates a derivative along a characteristic of slope U_o (particle path). If the length ξ is introduced and defined as the distance that a particle in the perfect fluid has traveled since its acceleration from rest by either the expansion wave or shock wave, the terms of equations (1a) to (3a) may be evaluated as functions of ξ alone in either region α or β. (See fig. 1.) It should be noted that the functional relationship may be different for the different regions. When these assumptions, together with the definition of ξ, are applied to the region α between the expansion zone and the entropy discontinuity, the following relations are obtained from the plot of distance against time of figure 1:

$$x = -a_\epsilon t_i + U_o(t - t_i) \tag{4}$$

$$\xi = U_o(t - t_i) \tag{5}$$

Substituting equation (4) into equation (5) gives

$$\xi = \frac{U_o}{U_o + a_\epsilon}(x + a_\epsilon t) \tag{6}$$

Therefore

$$\frac{\partial(\ )}{\partial x} = \frac{d(\ )}{d\xi}\frac{\partial\xi}{\partial x} = \frac{U_o}{U_o + a_\epsilon}\frac{d(\ )}{d\xi} \tag{7a}$$

and

$$\frac{\partial(\ )}{\partial t} = \frac{d(\ )}{d\xi}\frac{\partial\xi}{\partial t} = \frac{a_\epsilon}{U_o + a_\epsilon}\frac{d(\ )}{d\xi} \tag{7b}$$

Equations (7a) and (7b) may be used to obtain the convective derivative as follows:

$$\frac{D(\ )}{Dt} = \frac{\partial(\ )}{\partial t} + U_o\frac{\partial}{\partial x} = U_o\frac{d(\ )}{d\xi} \tag{8}$$

and since the characteristic derivative is expressed as

$$\frac{\delta(\ )}{\delta t} = \frac{D(\ )}{Dt} \pm a_\alpha \frac{\partial(\ )}{\partial x} \tag{9}$$

this derivative may be written, for region α of figure 1, by substituting equations (7a) and (8) into equation (9) as

$$\left.\begin{aligned}\frac{\delta(\ )}{\delta t} &= U_o \frac{d(\ )}{d\xi} \pm \frac{U_o}{U_o + a_\epsilon} a_\alpha \frac{d(\ )}{d\xi}\\ \frac{\delta(\ )}{\delta t} &= \frac{M_\alpha + \eta \pm 1}{M_\alpha + \eta} U_o \frac{d(\ )}{d\xi}\end{aligned}\right\} \tag{10}$$

Similarly, for region β, which lies between the entropy discontinuity and the shock wave,

$$\frac{\delta(\ )}{\delta t} = \frac{\sigma M_s - M_\beta \mp 1}{\sigma M_s - M_\beta} U_o \frac{d(\ )}{d\xi} \tag{11}$$

When equations (3a), (8), (10), and (11) are substituted in equations (1a) and (2a) and the area term is neglected because of the averaging process described in appendix A, the following equations are found for regions α and β, respectively. In order to avoid needless repetition, the solutions for both $\delta P/\delta t$ and $\delta Q/\delta t$ are presented in one equation with both plus and minus signs indicated for certain terms on the right-hand side. The upper signs apply to the characteristics with slope $U + a$ and the lower signs to those with slope $U - a$. Thus,

$$\begin{aligned}\frac{1}{a_\epsilon}\begin{Bmatrix}\dfrac{\delta P}{\delta t}\\[2ex] \dfrac{\delta Q}{\delta t}\end{Bmatrix}_\alpha &= \frac{2}{D}\frac{1}{\eta}\left\{\left[(\gamma - 1)M_\alpha \mp 1\right]M_\alpha + \frac{M_\alpha + \eta \pm 1}{M_\alpha + \eta}M_\alpha^2 + \right.\\ &\qquad \left.\frac{\theta_\alpha}{T_\alpha}P_r^{-2/3}\left[1 + \frac{M_\alpha + \eta \pm 1}{(M_\alpha + \eta)(\gamma - 1)}\right]\right\}Uc_{f_\alpha}\\ &= \begin{Bmatrix}\phi_{P_\alpha}\\ \phi_{Q_\alpha}\end{Bmatrix}\frac{U}{D}c_{f_\alpha}\end{aligned} \tag{12}$$

$$\frac{1}{a_\epsilon}\left\{\begin{matrix}\dfrac{\delta P}{\delta t}\\ \\ \dfrac{\delta Q}{\delta t}\end{matrix}\right\}_\beta = \frac{2}{D}\frac{a_\beta}{a_\epsilon}\left\{\left[(\gamma - 1)M_\beta \mp 1\right]M_\beta + \frac{\sigma M_s - M_\beta \mp 1}{\sigma M_s - M_\beta}M_\beta{}^2 + \frac{\theta_\beta}{T_\beta}P_r{}^{-2/3}\left[1 + \frac{\sigma M_s - M_\beta \mp 1}{(\gamma - 1)\left(\sigma M_s - M_\beta\right)}\right]\right\}Uc_{f_\beta}$$

$$= \left\{\begin{matrix}\phi_{P_\beta}\\ \\ \phi_{Q_\beta}\end{matrix}\right\}\frac{U}{D}c_{f_\beta} \tag{13}$$

These equations may be integrated along the characteristic lines. However, for ease of computation, since the slopes of these lines are assumed constant for each region due to the linearization process, integration may proceed along particle paths by a suitable change of variable. For example, from the geometry of the accompanying sketch of region α, the following equations apply:

$$x(t) = -a_\epsilon t_i + U(t - t_i)$$

$$x(t) = -a_\epsilon t_b + (U + a_\alpha)(t - t_b)$$

$$x(t) = Ut_d + (U - a_\alpha)(t - t_d)$$

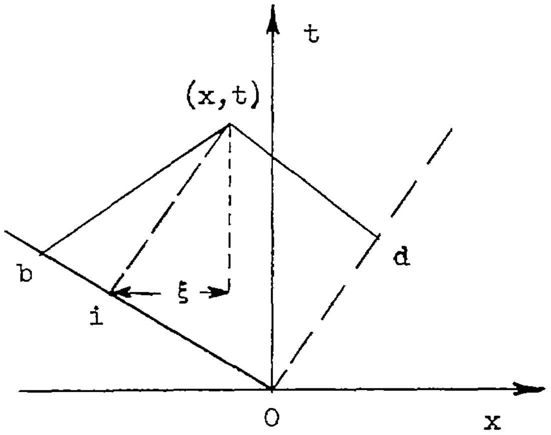

Solutions of the first and second equations and of the first and third equations yield

$$(t - t_i) = \frac{U + a_\alpha + a_\epsilon}{U + a_\epsilon}(t - t_b)$$

and

$$(t - t_i) = \frac{U + a_\epsilon - a_\alpha}{U + a_\epsilon}(t - t_d) + t_d$$

Therefore, from the definition of the length ξ in region α as $\xi = U(t - t_i)$, the following relations are obtained:

Along tt_b,

$$\xi = (t - t_b)U \frac{1 + M_\alpha + \eta}{M_\alpha + \eta} \tag{14}$$

$$\delta t = \frac{d\xi}{U} \frac{M_\alpha + \eta}{1 + M_\alpha + \eta} \tag{15}$$

Along tt_d,

$$\xi = (t - t_d)U \frac{M_\alpha + \eta - 1}{M_\alpha + \eta} + Ut_d \tag{16}$$

$$\delta t = \frac{d\xi}{U} \frac{M_\alpha + \eta}{M_\alpha + \eta - 1} \tag{17}$$

Therefore equation (12) is integrated in region α with the change of variable specified in equations (14) to (17):

$$\frac{P_t - P_b}{a_\epsilon} = \frac{1}{a_\epsilon} \int_{t_b}^{t} \left(\frac{\delta P}{\delta t}\right)_\alpha \delta t = \frac{\phi P_\alpha}{D} \int_{t_b}^{t} Uc_{f_\alpha} \delta t$$

or

$$\frac{P_t - P_b}{a_\epsilon} = \frac{\phi P_\alpha}{D} \frac{M_\alpha + \eta}{M_\alpha + \eta + 1} \int_0^{\xi(t)} c_{f_\alpha}\, d\xi \tag{18}$$

and

$$\frac{Q_t - Q_d}{a_\epsilon} = \frac{1}{a_\epsilon}\int_{t_d}^{t}\left(\frac{\delta Q}{\delta t}\right)_\alpha \delta t$$

or

$$\frac{Q_t - Q_d}{a_\epsilon} = \frac{\phi_{Q_\alpha}}{D}\,\frac{M_\alpha + \eta}{M_\alpha + \eta - 1}\int_{Ut_d}^{\xi(t)} c_{f_\alpha}\, d\xi \qquad (19)$$

Similar relationships may be found for region β. From the geometry of the accompanying sketch, it is evident that x may be expressed as follows:

$$x(t) = U_s t_j + U\left(t - t_j\right)$$

$$x(t) = U t_f + \left(U + a_\beta\right)\left(t - t_f\right)$$

$$x(t) = U_s t_k + \left(U - a_\beta\right)\left(t - t_k\right)$$

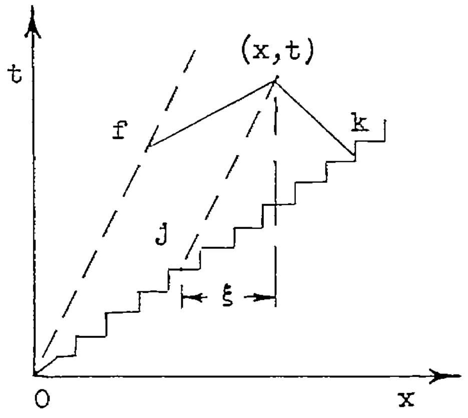

Solving the above equations yields

$$t - t_j = \frac{a_\beta\left(t - t_f\right)}{U - U_s} + t$$

and

$$t - t_j = \frac{U_s - U + a_\beta}{U_s - U}\left(t - t_k\right)$$

Consequently, since in region β, $\xi = U\left(t - t_j\right)$, the following relations apply:

Along $t_f t$,

$$\xi = \frac{\sigma M_s - M_\beta - 1}{\sigma M_s - M_\beta} U\left(t - t_f\right) + Ut_f \tag{20}$$

$$\delta t = \frac{d\xi}{U} \frac{\sigma M_s - M_\beta}{\sigma M_s - M_\beta - 1} \tag{21}$$

and along tt_k,

$$\xi = \frac{1 + \sigma M_s - M_\beta}{\sigma M_s - M_\beta} U\left(t - t_k\right) \tag{22}$$

$$\delta t = \frac{d\xi}{U} \frac{\sigma M_s - M_\beta}{1 + \sigma M_s - M_\beta} \tag{23}$$

Therefore, equations (13) and (20) to (23) can be used to obtain

$$\frac{P_t - P_f}{a_\epsilon} = \int_{t_f}^{t} \frac{1}{a_\epsilon}\left(\frac{\delta P}{\delta t}\right)_\beta \delta t = \frac{\phi_{P_\beta}}{D} \int_{t_f}^{t} Ucf_\beta \delta t$$

$$= \frac{\phi_{P_\beta}}{D} \frac{\sigma M_s - M_\beta}{\sigma M_s - M_\beta - 1} \int_{Ut_f}^{\xi(t)} cf_\beta \, d\xi \tag{24}$$

and

$$\frac{Q_t - Q_k}{a_\epsilon} = \int_{t_k}^{t} \frac{1}{a_\epsilon}\left(\frac{\delta Q}{\delta t}\right)_\beta \delta t = \frac{\phi_{Q_\beta}}{D} \int_{t_f}^{t} Ucf_\beta \delta t$$

$$= \frac{\phi_{Q_\beta}}{D} \frac{\sigma M_s - M_\beta}{\sigma M_s - M_\beta + 1} \int_{0}^{\xi(t)} cf_\beta \, d\xi \tag{25}$$

The entropy at any point (x,t) in region α or β may be found simply by integration along a particle path (since ξ is the product of U multiplied by flow time, $d\xi = U\,dt$), so that from equation (3a),

$$\left.\begin{aligned}\frac{S_t - S_b}{R}\\ \frac{S_t - S_j}{R}\end{aligned}\right\} = \int_0^t \left(\frac{D\frac{S}{R}}{Dt}\right)_{\substack{\alpha\\ \beta}} dt = \frac{2\gamma}{D}\left[M_{\substack{\alpha\\ \beta}}^{\ 2} + \frac{1}{\gamma - 1}\left(\frac{\theta}{T}\,P_r^{\ -2/3}\right)_{\substack{\alpha\\ \beta}}\right]\int_0^{\xi(t)} c_{f_{\substack{\alpha\\ \beta}}}\,d\xi$$

$$= \frac{1}{D}\,\phi_{s_{\substack{\alpha\\ \beta}}}\int_0^{\xi(t)} c_{f_{\substack{\alpha\\ \beta}}}\,d\xi \tag{26}$$

It is now necessary to consider the transmission and reflection of the characteristics at the entropy discontinuity separating the fluid which was initially at a high pressure behind the diaphragm from that which was initially at a low pressure ahead of the diaphragm. These effects are important, even in a linearized solution, because of the large differences in ν which may exist in the fluids on each side of the discontinuity.

If the subscript o refers to conditions in a perfect fluid (that is, immediately after diaphragm burst in real fluid) and the notation of figure 1 is followed, it is shown in appendix C that, if $\lambda \ll 1$ and γ is the same in both α and β,

$$\frac{\Delta S}{R} = \frac{S_f - S_c}{R} = \frac{\Delta S_o}{R}(1 + \lambda) = \left(\frac{S_\beta - S_\alpha}{R}\right)_o (1 + \lambda) \tag{27}$$

Then,

$$\frac{\delta P}{\delta P_o} = \frac{P_f - P_c}{P_{\beta_o} - P_{\alpha_o}} = \frac{\delta Q}{\delta Q_o} = \frac{Q_f - Q_c}{Q_{\beta_o} - Q_{\alpha_o}}$$

$$= 1 + \frac{P_c - P_{\alpha_o} + Q_f - Q_{\beta_o}}{P_{\alpha_o} + Q_{\beta_o}} + \frac{\gamma - 1}{\gamma}\,\frac{a_{\beta_o}/a_{\alpha_o}}{\left(\frac{a_{\beta_o}}{a_{\alpha_o}}\right)^2 - 1}\left[\frac{S_f - S_{\beta_o}}{R} - \frac{S_c - S_{\alpha_o}}{R}\right] \tag{28}$$

The second term on the right-hand side indicates the change in the characteristic value which would occur as a result of reflections and refractions even without any change in entropy. The third term evaluates the additional variation due to the changing entropy.

The reflections at the shock wave of the incident waves are of higher order and may be ignored in this solution.

The following equations result from the definition of P, Q, and S/R and subsequent linearization with the limitation to small perturbations:

$$\frac{a}{a_\epsilon} = \frac{\gamma - 1}{4} \frac{P + Q}{a_\epsilon} \tag{29}$$

$$\frac{U}{a_\epsilon} = \frac{P - Q}{2a_\epsilon} \tag{30}$$

$$\begin{aligned}
\frac{p}{p_o} &= \left(\frac{a}{a_o}\right)^{\frac{2\gamma}{\gamma-1}} e^{-\frac{S-S_o}{R}} \\
&= \left(1 + \frac{a - a_o}{a_o}\right)^{\frac{2\gamma}{\gamma-1}} e^{-\frac{S-S_o}{R}} \\
&\approx \left(1 + \frac{2\gamma}{\gamma - 1} \frac{a - a_o}{a_o}\right)\left(1 - \frac{S - S_o}{R}\right) + \dots \\
&\approx 1 + \frac{2\gamma}{\gamma - 1} \frac{a - a_o}{a_o} - \frac{S - S_o}{R} + \dots \\
&\approx 1 + \frac{\gamma}{2} \frac{a_\epsilon}{a_o}\left(\frac{P - P_o + Q - Q_o}{a_\epsilon}\right) - \frac{S - S_o}{R} + \dots
\end{aligned} \tag{31}$$

$$\frac{\rho}{\rho_o} = \left(\frac{a}{a_o}\right)^{\frac{2}{\gamma-1}} e^{-\frac{S-S_o}{R}}$$

$$\approx 1 + \frac{1}{2}\frac{a_\epsilon}{a_o}\left(\frac{P - P_o + Q - Q_o}{a_\epsilon}\right) - \frac{S - S_o}{R} + . \; . \; . \; . \; . \tag{32}$$

Consequently, the description of the flow at any desired distance and time may be determined by combining equations (29) to (32) with equations (18), (19), (24), (25), (26), and (28) with the proper limits of integration determined by geometry on the x,t plot.

It is to be noted that the values of P, Q, and S/R must also be determined at the intersection of the entropy discontinuity with the characteristic passing through the point (v or w) at which the flow properties are to be determined. This step is required to compute the transmission and reflections of the characteristic parameters as determined by equation (28).

In region α at the point $x_w = Wt_w = M_w a_\epsilon t_w$ (see fig. 1), the equations become:

$$\frac{P_w - P_b}{a_\epsilon} = \phi_{P_\alpha} \frac{1}{D} \frac{M_\alpha + \eta}{M_\alpha + \eta + 1} \int_0^{\frac{M_w+1}{M_\alpha+\eta}\eta U t_w} c_{f_\alpha} \, d\xi \tag{33}$$

$$\frac{P_d - P_q}{a_\epsilon} = \phi_{P_\alpha} \frac{1}{D} \frac{M_\alpha + \eta}{M_\alpha + \eta + 1} \int_0^{\left(1+\eta M_w - M_\alpha\right)U t_w} c_{f_\alpha} \, d\xi \tag{34}$$

$$\frac{Q_e - Q_m}{a_\epsilon} = \frac{Q_e - Q_{\beta_o}}{a_\epsilon} = \phi_{Q_\beta} \frac{1}{D} \frac{\sigma M_s - M_\beta}{\sigma M_s - M_\beta + 1} \int_0^{\left(1+\eta M_w - M_\alpha\right)U t_w} c_{f_\beta} \, d\xi \tag{35}$$

$$\frac{Q_w - Q_d}{a_\epsilon} = \phi_{Q_\alpha} \frac{1}{D} \frac{M_\alpha + \eta}{M_\alpha + \eta - 1} \int_{\left(1+\eta M_w - M_\alpha\right)U t_w}^{\frac{M_w+1}{M_\alpha+\eta}\eta U t_w} c_{f_\alpha} \, d\xi \tag{36}$$

$$\frac{S_w - S_i}{R} = \phi_{s_\alpha} \frac{1}{D} \int_0^{\frac{M_w+1}{M_\alpha+\eta}\eta U t_w} c_{f_\alpha}\, d\xi \tag{37}$$

$$\frac{Q_d - Q_e}{Q_{\alpha_o} - Q_{\beta_o}} = 1 + \frac{\left(P_d - P_q\right) + \left(Q_e - Q_m\right)}{P_{\alpha_o} + Q_{\beta_o}} +$$

$$\frac{\gamma - 1}{\gamma} \frac{a_{\beta_o}/a_{\alpha_o}}{\left(\frac{a_{\beta_o}}{a_{\alpha_o}}\right)^2 - 1} \frac{1}{D}\left[\phi_{s_\beta} \int_0^{\left(1+\eta M_w-M_\alpha\right)Ut_w} c_{f_\beta}\, d\xi \right. -$$

$$\left. \phi_{s_\alpha} \int_0^{\left(1+\eta M_w-M_\alpha\right)Ut_w} c_{f_\alpha}\, d\xi \right] \tag{38}$$

It should be noted that the neglect of the expansion fan in the derivation is reflected in the term $1 + \eta M_w - M_\alpha$ appearing in the limits of integration of the above equations. Values of M_w such that the point w is in the expansion fan make the factor $1 + \eta M_w - M_\alpha$ negative and give only meaningless answers.

Equations similar to those for region α are obtained for region β at $x_v = Vt_v = M_v a_\infty t_v$ as follows:

$$\frac{P_c - P_b}{a_\epsilon} = \phi_{P_\alpha} \frac{1}{D} \frac{M_\alpha + \eta}{M_\alpha + \eta + 1} \int_0^{\left(1+M_\beta-\sigma M_v\right)Ut_v} c_{f_\alpha}\, d\xi \tag{39}$$

$$\frac{P_v - P_f}{a_\epsilon} = \phi_{P_\beta} \frac{1}{D} \frac{\sigma M_s - M_\beta}{\sigma M_s - M_\beta - 1} \int_{\left(1+M_\beta-\sigma M_v\right)Ut_v}^{\frac{M_s-M_v}{\sigma M_s-M_\beta}\sigma U t_v} c_{f_\beta}\, d\xi \tag{40}$$

$$\frac{Q_f - Q_g}{a_\epsilon} = \phi_{Q_\beta} \frac{1}{D} \frac{\sigma M_s - M_\beta}{\sigma M_s - M_\beta + 1} \int_0^{\left(1+M_\beta-\sigma M_v\right)Ut_v} c_{f_\beta}\, d\xi \tag{41}$$

$$\frac{Q_v - Q_k}{a_\epsilon} = \frac{Q_v - Q_{\beta_o}}{a_\epsilon} = \phi_{Q_\beta} \frac{1}{D} \frac{\sigma M_s - M_\beta}{\sigma M_s - M_\beta + 1} \int_0^{\frac{M_s - M_v}{\sigma M_s - M_\beta} \sigma U t_v} c_{f_\beta} \, d\xi \tag{42}$$

$$\frac{P_f - P_c}{P_{\beta_o} - P_{\alpha_o}} = 1 + \frac{\left(P_c - P_b\right) + \left(Q_f - Q_g\right)}{P_{\alpha_o} + Q_{\beta_o}} + \frac{(\gamma - 1)}{\gamma} \frac{a_{\beta_o}/a_{\alpha_o}}{\left(\frac{a_{\beta_o}}{a_{\alpha_o}}\right)^2 - 1} \frac{1}{D}\left[\phi_{s_\beta} \int_0^{\left(1+M_\beta-\sigma M_v\right) U t_v} c_{f_\beta} \, d\xi - \phi_{s_\alpha} \int_0^{\left(1+M_\beta-\sigma M_v\right) U t_v} c_{f_\alpha} \, d\xi\right] \tag{43}$$

$$\frac{S_v - S_j}{R} = \frac{S_v - S_{\beta_o}}{R} = \frac{1}{D} \phi_{s_\beta} \int_0^{\frac{M_s - M_v}{\sigma M_s - M_\beta} \sigma U t_v} c_{f_\beta} \, d\xi \tag{44}$$

The solution to the small-perturbation problem of shock-tube flow has now been reduced to the evaluation of integrals of the form $\int c_f(\xi) d\xi$ where ξ is simply a length formed by the product of the flow time multiplied by the fluid velocity. Any analytic or graphical method giving c_f as a function of ξ may be used in the evaluation of these integrals.

In order to evaluate equations (33) to (44), it is necessary to know the state of the boundary layer at a point in the shock tube which is denoted by a corresponding point $\xi(x,t)$ of the characteristics diagram. The boundary-layer problem is a "hybrid" of the Rayleigh problem of the instantaneous acceleration of a flat plate and the Blasius problem of the steady flow over a semi-infinite flat plate. It is similar to the Rayleigh problem in that, at a given instant of time, all the flow between the shock and expansion wave has been accelerated from zero velocity to a constant velocity but is different from the Rayleigh problem in that the fluid has been in motion for varying time durations. It is similar to the Blasius problem in that, along a particle path in x,t coordinates, the boundary layer increases rearward from the shock or "leading edge," but is different in that the leading edge is not stationary. A solution to this hybrid problem for laminar boundary layers was found in reference 3 for region β by reducing the unsteady-flow problem to a steady-flow problem by choosing a coordinate system fixed to the shock wave. The problem then became the Blasius problem modified for a nonzero wall velocity. In a similar manner a solution could be found for region α if the expansion wave were assumed to have zero thickness and the coordinate system were fixed to the leading edge of the expansion wave.

For laminar flows, the solutions to the Rayleigh problem, the Blasius problem, and the modified Blasius problem of reference 3 all show the skin friction to be inversely proportional to the square root of the time that a fluid particle in the free stream outside the boundary layer has been in motion over the plate. It should be noted that the constants of proportionality are different in each of the above cases. No solutions to the turbulent-boundary-layer equivalent of the Rayleigh or modified Blasius problem are known to the authors. One might assume, however, that the state of the boundary layer at a point in a turbulent flow (as well as in a laminar flow) over a flat plate with zero pressure gradient may be expressed as a function of the time interval that the fluid has been in motion over the flat plate or of the distance the outer fluid has moved along the plate.

In the absence of a modified Blasius solution in region α and of any solution whatsoever for the analogous problem of turbulent-boundary-layer flow in either α or β, an approximate method of evaluation for the integrals may be obtained by extending the above-mentioned time-dependency assumption further and assuming that the linearized unsteady flow in a shock tube has the same properties as an equivalent steady flow defined in the following manner: The properties of a lamina of fluid in the shock tube which has been in motion with a velocity U_o for a time t are equivalent to those of a lamina of fluid which has progressed rearward for a period of time t from the leading edge of a semi-infinite flat plate in a steady flow with free-stream velocity U_o. Under these conditions ξ becomes the distance from the leading edge of the flat plate.

The introduction of this assumption reduces the small-perturbation solution to the simple evaluation of the integral of the skin-friction distribution along a semi-infinite flat plate in steady flow. This integral may be evaluated if the relationship between c_f and ξ is prescribed either in analytic form or as a curve of c_f plotted against ξ or of c_f against R_e. The former method of relationship will usually permit evaluation of the integral in closed form, whereas the latter method may require graphical integration.

A theory has now been obtained for small-perturbation flow in a shock tube with the following assumptions:

(1) Variations from perfect fluid flow shall be small.

(2) Averaged values are used for quasi-one-dimensional flow.

(3) Averaged values of ρ and U which identically satisfy the continuity equation are also assumed to satisfy the momentum equation.

(4) The frictional dissipation is approximated as the product of the average velocity times the wall-shearing force.

(5) The perfect-fluid characteristic net, velocities, densities, and so forth are used to obtain linearized values.

(6) The expansion fan is treated as a "negative shock wave" in that the final values of velocity, pressure, and so on, are assumed to exist immediately after the leading edge of the expansion fan.

(7) If numerical evaluation of the theory is performed on the basis of equivalent-flat-plate steady flow, the following assumptions are also introduced:

> (a) The steady and unsteady skin frictions are equal for a fluid which has traveled a given distance over a flat plate in steady flow and for a fluid which has traveled the same distance along the shock tube in unsteady flow.
>
> (b) The boundary layer is small relative to the width or height of the shock tube.

EXPERIMENTAL APPARATUS AND PROCEDURE

Experiments to determine the validity of the theory were performed in a high-pressure shock tube 2 inches high by $1\frac{1}{2}$ inches wide in the Langley gas dynamics laboratory. Air at room temperature was used for both high- and low-pressure sections of the shock tube. Measurements of shock velocity and pressure-time variation were taken at various points along the shock tube.

The low-pressure side of the shock tube was at room conditions; whereas the high-pressure chamber was filled to pressures of 45, 70, 95, or 250 pounds per square inch gage. Either one or two sheets of soft brass shim stock 0.00125 or 0.0015 inch thick was employed as a diaphragm. The number and thickness of the brass sheets were determined so that the diaphragm was near its breaking stress at the particular pressures of the test. Consequently, optimum diaphragm burst would result when the point of the rupturing mechanism pierced the center of the diaphragm. It has been found that imperfect diaphragm bursts will result in both increased shock attenuation and scatter of experimental data.

The shock velocity was measured at distances of 3.23, 5.23, 7.23, 9.18, and 11.18 feet from the diaphragm by inserting shock-tube sections of various length between the diaphragm and the glass-walled test section. A block diagram of the experimental apparatus is shown in figure 2. Velocity was determined from measurements of the time required for the shock wave to traverse the 1.206 feet between the two light beams of the optical systems. (See figs. 2 and 3.) Each optical system consisted of a direct-current automobile lamp with line filament alined vertically at the focal point of a two-inch-diameter, seven-inch focal-length lens. The light emitted from the lens was masked to a vertical slit approximately 0.030 inch wide and 1 inch high. Stray light on the upstream side of this beam was cut off with a sharp knife edge. The beam then passed perpendicularly through the test-section window and impinged on the edge of a second knife edge about ten inches from the test-section window. When the plane shock wave reached the upstream edge of each beam, light was refracted off the second knife edge onto a phototube. The resulting signal of each phototube was amplified by the circuit shown in figure 4. The output pulse from each thyratron (2D21) was used to trigger one channel of an eight-megacycle counter chronograph. The pulse from the upstream system triggered the chronograph "start" circuit and that from the downstream system, the "stop" circuit. (See fig. 2.) The time interval could thus be measured to within ±1/8 microsecond.

Pressure-time records were obtained for the four nominal pressure ratios at a distance of 8.13 feet from the diaphragm by employing a flush-mounted capacitor-type pressure pickup (Rutishauser Electronic Pickup Indicator, Type ST-127A) and associated apparatus, as shown schematically in figure 2. The signal from fluctuations on the pressure pickup was fed into the Y-axis of one beam of a four-channel cathode-ray oscillograph, and the resulting deflection of the beam was photographed by an NACA synchronous drum camera rotating at 1,800 rpm. A 1,000-cps sine-wave timing trace was fed into another channel of the oscillograph in order to obtain a time base.

The oscillograph beams could be turned on and off electronically by application of a suitable signal to the Z-axis of the oscillograph. This signal was obtained from a piezoelectric crystal pickup, a preamplifier, and an NACA electronic shutter circuit. (See fig. 2.) The crystal pickup was located 6.4 feet from the diaphragm so that the oscillograph would record the ambient pressure ("zero trace") before arrival of the shock wave. The time duration of the oscillograph trace was adjustable up to 20 milliseconds.

A minimum of five test runs was made for each combination of nominal pressure ratio and distance to the median position of the velocity-measuring system. The chronograph time interval, the shock-tube-wall temperature, and the barometric pressure were recorded for each test.

Pressure-time records at $x = 8.13$ feet were taken, along with simultaneous velocity measurements at a median position of 9.23 feet. The aforementioned data were recorded and, in addition, a static calibration of the pressure gage was performed for each run. This calibration was made by applying pressure to the shock tube in predetermined increments, and at each pressure level the oscillograph Z-axis was energized so that the static-pressure calibration trace of the gage could be photographed to place a pressure scale on the drum-camera-film record.

RESULTS AND DISCUSSION

Evaluation of Experimental Data

The experimental shock strengths shown in figure 5 were determined from the time interval Δt seconds for the shock to pass the slits of the measuring station a distance Δl feet apart as follows:

$$\frac{p_{v_s}}{p_\infty} = \frac{2\gamma}{\gamma + 1}\left(\frac{\Delta l/\Delta t}{a_\infty}\right)^2 - \frac{\gamma - 1}{\gamma + 1} \qquad (45)$$

which becomes, for $\gamma = 1.40$ and dry air,

$$\frac{p_{v_s}}{p_\infty} = \frac{4.859 \times 10^{-4}}{T_\infty}\left(\frac{\Delta l}{\Delta t}\right)^2 - 0.1667 \qquad (46)$$

The pressure was plotted at a value of x halfway between the phototubes.

The experimental data required some slight adjustment before it could be presented in figure 5, each part of which represents a common diaphragm pressure ratio or theoretical perfect-fluid shock pressure ratio. Since the tests pertinent to a given nominal diaphragm pressure ratio were made with the high-pressure chamber at the same gage pressure, variations in atmospheric pressure from time to time caused a variation in diaphragm pressure ratio. The required adjustment was made in accordance with the relations that follow (notation of fig. 1).

Since the equation relating shock pressure ratio to diaphragm pressure ratio (see refs. 3, 4, and 7) may be expressed in functional form as

$$\frac{p_\epsilon}{p_\infty} = f\left(\frac{p_\beta}{p_\infty}\right)_o \tag{47}$$

then

$$\frac{d\,\dfrac{p_\epsilon}{p_\infty}}{d\,\dfrac{p_\beta}{p_\infty}} = f'\left(\frac{p_\beta}{p_\infty}\right)_o \tag{48}$$

and

$$\left(\frac{p_\beta}{p_\infty}\right)_{\substack{\text{adjusted to} \\ \text{ref. } p_\epsilon/p_\infty}} = \left(\frac{p_\beta}{p_\infty}\right)_{exp} + \frac{1}{f'}\left[\left(\frac{p_\epsilon}{p_\infty}\right)_{ref} - \left(\frac{p_\epsilon}{p_\infty}\right)_{exp}\right] \tag{49}$$

The reference value of p_ϵ/p_∞ for each nominal diaphragm pressure ratio was taken as the value existing when the pressure-time records were obtained by the capacitor pickup.

Since each of the velocity symbols represents an average (on a given day) of from five to ten test runs, in which the scatter in any set taken on the same day is less than the scatter among averages of data taken on different days, the reason for the discrepancy between averages at the same distance and same theoretical pressure ratio is unknown. Temperature, viscosity, and humidity corrections, determined from the linear theory and applied to these experimental points, are insufficient to make the averages coincide. The cause of the apparently high experimental pressure ratio at $x = 3.2$ feet (fig. 5) is also unexplainable at present.

The pressure-time traces of the capacitor pickup located 8.13 feet from the diaphragm station are shown in figure 6. The linear-theory values computed at $x = 8.0$ feet are plotted (circled points) for comparison at millisecond intervals after the arrival of the shock. The shock pressure ratio obtained from concurrent velocity data for each particular run falls on the initial theoretical point within the accuracy of plotting. The velocity data, obtained at $x = 9.23$ feet, were adjusted to 8.13 feet by drawing a curve through the velocity point at 9.23 feet parallel to the experimental curves of figures 5(a) to 5(d); thereby compensation was provided for any scatter in the particular test.

Evaluation of Linear Theory

Constants employed.- The equations of the linear theory are evaluated on the assumption that standard atmospheric conditions exist in the low-pressure chamber unless specified otherwise. Temperature recovery factors r of 0.90 and 0.85 are used for the turbulent and laminar boundary layers, respectively. A Prandtl number P_r of 0.71 and a value of the Blasius constant B of 8.70 are assumed.

The temperature-viscosity relationship

$$\frac{\mu}{\mu_\infty} = \frac{T_\infty + 223.2}{T + 223.2}\left(\frac{T}{T_\infty}\right)^{1.5} \tag{50}$$

was expanded for computational convenience to give the approximation

$$\frac{\mu}{\mu_\infty} = \left(\frac{T}{T_\infty}\right)^{0.80} \tag{51}$$

which is considered valid in the temperature range near 520° Rankine.

Relation between $c_f(\xi)$ and ξ.- Various theoretical, empirical, and experimental relations are available for relating c_f to ξ for evaluation of the integral $\int c_f(\xi)d\xi$. If the assumption of an equivalent-flat-plate steady flow is employed and the boundary-layer profile obeys the law

$$\frac{u_y}{U} = \left(\frac{y}{\delta}\right)^{1/n} \tag{52}$$

it is shown in appendix D for an incompressible turbulent boundary layer and for n and B independent of ξ that

$$\left.\begin{aligned} c_f(\xi) &= 2\left[\frac{n}{(n+2)(n+3)B^n}\right]^{\frac{2}{n+3}}\left(\frac{\nu}{U\xi}\right)^{\frac{2}{n+3}} \\ c_f(\xi) &= N\left(\frac{\nu}{U\xi}\right)^{\frac{2}{n+3}} \end{aligned}\right\} \tag{53}$$

Then, the integral may be evaluated in closed form as

$$\int_{\xi_1}^{\xi_2} c_f \, d\xi = N\left(\frac{\nu}{U}\right)^{\frac{2}{n+3}} \frac{n+3}{n+1}\left[\xi^{\frac{n+1}{n+3}}\right]_{\xi_1}^{\xi_2} \tag{54}$$

Similarly, if the equivalent steady flow is used with an incompressible laminar boundary layer (see ref. 9), the solution is

$$c_f(\xi) = 0.664\left(\frac{\nu}{U\xi}\right)^{1/2} \tag{55}$$

$$\int_{\xi_1}^{\xi_2} c_f \, d\xi = 0.664\left(\frac{\nu}{U}\right)^{1/2} 2\left[\xi^{1/2}\right]_{\xi_1}^{\xi_2}$$

$$= 1.328\left(\frac{\nu}{U}\right)^{1/2}\left[\xi^{1/2}\right]_{\xi_1}^{\xi_2} \tag{56}$$

If the moving wall or modified Blasius solution of reference 3 is used, the expression for $c_f(\xi)$ in region β reduces to

$$c_f(\xi) = -\frac{A_2}{A_1}\frac{U_s}{U}\left(\frac{\nu}{U\xi}\right)^{1/2} \tag{57}$$

in which A_2/A_1 are constants evaluated in reference 3. Then

$$\int_{\xi_1}^{\xi_2} c_f(\xi)d\xi = -2\left(\frac{A_2}{A_1}\right)\frac{U_s}{U}\left(\frac{\nu}{U}\right)^{1/2}\left[\xi^{1/2}\right]_{\xi_1}^{\xi_2} \tag{58}$$

Since reference 3 does not consider region α, no equivalent expression for this region is available. However, if the same general assumptions were applied to region α as were applied to region β, evaluations of $c_f(\xi)$ would again yield an equation in which $c_f(\xi)$ is proportional to $\left(\frac{\nu}{U\xi}\right)^{1/2}$.

In order to determine a possible correct relationship between $c_f(\xi)$ and ξ to be used in evaluating the linear theory for the range of experiments covered in this paper, the curves of theoretical and experimental shock pressure ratio against distance of figure 5(c) were used. In addition to the experimental points obtained for a nominal diaphragm pressure ratio of 7.455 (shock pressure ratio 2.523), theoretical curves are plotted by assuming an equivalent steady flow for (a) laminar skin friction $\left(c_f = 0.664R_e^{-1/2}\right)$; (b) turbulent skin friction $\left(c_f = 0.0581R_e^{-1/5},\ n = 7\right)$ with and without heat-transfer effects; and (c) an experimental curve (from fig. 88 of ref. 10) giving the integrated value of c_f, which includes the effect of transition of the boundary layer from laminar to turbulent. Since, as mentioned previously, the modified laminar Blasius solution of reference 3 was not evaluated in region α, no theoretical curve can be drawn for the corresponding $c_f(\xi)$. However, due to the laminar assumptions of reference 3, the attenuation in shock pressure ratio would be proportional to $\sqrt{x}$ if $c_f(\xi)$ were evaluated in region α with similar assumptions to those used for region β. Consequently, in order to determine whether such a modified Blasius treatment could possibly yield the correct relation between c_f and ξ, a curve of the type $\frac{p_{v_s}}{p_\infty} = \frac{p_{\beta_o}}{p_\infty} - (\text{Constant})\sqrt{x}$ was fitted to the experimental data at $x = 9$ feet and the constant was found to be 0.0626. This resulting empirical curve, $\frac{p_{v_s}}{p_\infty} = 2.523 - 0.0626\sqrt{x}$, is also plotted in figure 5(c).

It is evident from an inspection of figure 5(c) that best agreement between theory and experiment is obtained either from the turbulent skin-friction law including heat-transfer effects or from the experimentally determined skin-friction curve of reference 10. The reason for the similarity of the shock pressure curves obtained by these two methods is simply that, for $R_e < 20 \times 10^6$, the turbulent skin-friction law $\left(c_f = 0.0581R_e^{-1/5}\right)$ for a value of $n = 7$ when integrated closely approximates the curve in reference 10 except at low values of R_e, where the laminar and transition effects are apparent. These latter effects result in the inflection in figure 5(c) of the curve based on the drag curve from reference 10. Inasmuch as these two skin-friction curves result in almost the same theoretical shock-pressure attenuation, either could be used for further evaluation of the theory. However, since an analytic closed-form integral is more convenient for computation in this case, the skin-friction law $c_f = 0.0581\left(\frac{U\xi}{\nu}\right)^{-1/5}$ was used for evaluation of the linear theory for the other figures in this paper.

It is also evident from figure 5(c) that the equivalent steady-flow laminar-boundary-layer skin friction predicts shock attenuation much less than that measured. Furthermore, the empirical curve (attenuation proportional to $\sqrt{x}$) - which might be said to represent the shape of laminar solutions in general, including the modified Blasius solution - does not indicate the trend of measured shock attenuation. Thus, it might be inferred from these conditions that the boundary layer is turbulent in most of the shock-tube-flow regions α and β at these values of R_e.

Comparison of Theory and Experiment

Shock attenuation with distance from diaphragm.- The theoretical shock pressure loss and shock attenuation coefficients are presented as functions of perfect-fluid shock pressure ratios in figure 7. These relations are used to predict the attenuation of the shock with distance traversed from the diaphragm station in figure 5 and the theoretical results are found to be in good agreement with the experimental data. Although the theoretical points are computed for standard atmospheric conditions, the experimental points are adjusted to the nonstandard atmospheric conditions existing when the pressure-time runs were made. In order to determine the magnitude of error so introduced, the theory was evaluated for the nonstandard ($T = 542^\circ$, $p = 14.7$ lb/sq in.) conditions for the diaphragm pressure ratio of 17.915 where the error introduced would be largest. The adjusted theory indicated by the dashed curve of figure 5(d) shows a slight increase in attenuation which agrees somewhat better with experiment than the "standard atmosphere" theory. The adjustment for nonstandard conditions would be even less for the other pressure ratios. (See fig. 7(b).)

Use of the linear theory with a value of $c_f = 0.0581R_e^{-1/5}$ appears in figure 5 to overestimate the attenuation slightly at the lower shock pressure ratios (below 2.5) with the opposite effect apparent at higher ratios. This trend could be due to any of a number of simplifications made in the theory and computations. Two of the more obvious factors are the Reynolds number and compressibility effects. As the diaphragm pressure ratio increases, the Reynolds number of the flow per unit length increases. Since, for the computations of this analysis, c_f is assumed proportional to $R_e^{-2/(n+3)}$ $\left(\text{which is equal to } R_e^{-1/5} \text{ for } n = 7\right)$ and since steady-flow experiments in general indicate a trend of c_f proportional to smaller negative powers (larger n) with R_e increasing, there is the possibility that values of n should be increasing somewhat with R_e and diaphragm pressure ratio. Compressibility would tend to reduce the ratio of the compressible c_f to the incompressible c_f and consequently would tend to reduce the attenuation as the flow Mach numbers increased with diaphragm pressure ratio.

The neglect of the spreading of the expansion fan must also be considered, since this omission must introduce an error which increases with shock pressure ratio (expansion-fan size).

Other possible factors open to question are the use of constant P_r, the evaluation of heat transfer on the basis of ν of the fluid in the center of the flow (for example, not at some intermediate temperature between the wall and stream), and the use of $r = 0.90(0.85)$. However, because of the assumptions in the one-dimensional averaging process, in the linearization procedure, and in the application of an equivalent steady-flow boundary layer, these points are minor refinements to the theory in the experimental range considered. Nevertheless, suitable corrections should be applied as higher diaphragm pressures are used if good correlation is desired.

The curves of figure 7, which were computed on a basis of $a_\epsilon = a_\infty$ and $c_f = 0.0581R_e^{-1/5}$, summarize shock attenuation prediction by the linear theory for shock pressure ratios up to 10. For c_f proportional to $R_e^{-2/(n+3)}$ this curve is of the type

$$\frac{\Delta p}{p_\infty} = \left[g\left(n, \frac{p_\beta}{p_\infty}\right)\right]\left(\frac{\nu_\infty}{a_\infty}\right)^{\frac{2}{n+3}} \frac{(l)^{\frac{n+1}{n+3}}}{D} \tag{59}$$

where Δp is the shock-pressure attenuation at a distance l from the diaphragm station. According to this equation the attenuation at a constant number of hydraulic diameters from the diaphragm would vary as the shock-tube Reynolds number $\left(\frac{a_{\infty}D}{\nu_{\infty}}\right)^{-\frac{2}{n+3}}$. This relationship is discussed more fully in a subsequent paragraph.

Variation of pressure with time at a given distance.- Pressure-time curves obtained experimentally by the capacitor pickup located a distance of 8.13 feet from the diaphragm station are compared in figure 6 with theoretical results computed (see fig. 8) for a distance of 8 feet and $c_f = 0.0581R_e^{-1/5}$. The error introduced by the variation in distance is about 1 percent of the attenuation pressure change and may be ignored. The experimental shock pressure was also obtained for each run by computing the pressure at 9.23 feet from simultaneous velocity measurements and then interpolating back to 8 feet along a curve parallel to the experimental curve of attenuation against distance. These velocity measurements fall on the theoretical measurements within the accuracy of the plotting of figure 6.

Both theoretical and experimental curves show a pressure increasing with time. This increase has also been noted when NACA miniature electrical pressure gages, as well as piezoelectric pressure pickups, have been employed. The initial pressure rise across the shock determined from the velocity measurements, as well as from the theory, appears to fall below the average of the initial damped high-frequency oscillations of the condenser pickup pressure-time curve. However, the dynamic response of the Rutishauser system is not known, whereas the shock-velocity measuring system has a known high precision. Consequently, the use of the initial shock-velocity pressure point in conjunction with the Rutishauser records, after the high-frequency oscillations have subsided, appears a logical choice to give a better representation of the actual pressure-time phenomena. Such an "experimental" curve agrees very favorably with the pressure rise predicted by the linear theory.

Variation of other parameters with time at a given distance.- Figures 9 to 12 show the predicted variation with time of average sonic speed, fluid velocity, density, and Mach number at $x = 8$ feet. The change of these parameters with time increases with shock strength, since the skin friction and the temperature difference between walls and fluid increase with shock strength for low values of shock pressure ratios. These aforementioned quantities were not measured in the experiments of this investigation; however, the phenomena of density increasing with time were found experimentally by the use of a chrono-interferometer and are reported in reference 8. The behavior of the average particle velocity has not been ascertained. An increase in speed of the leading edge of the mixing zone which replaces the entropy discontinuity between the hot and cold gas regions of the theoretical flow has been reported in reference 7 and elsewhere. However, the apparent velocity increase of the leading edge is also attributable to turbulent mixing since it is known that the width of the zone increases with time. Consequently, the velocity of the leading edge does not give a true indication of the average particle velocity due to the masking effect of mixing. An increase in Mach number with time was found experimentally in reference 3. Also, an attempt to measure sound speed was reported in reference 3, but the reported result of constant sound speed with ±2 percent variation over a 100-microsecond interval does not appear significant in view of the procedure employed and, in addition, the predicted linear-theory variation (fig. 9) is less than scatter of the data of reference 3.

Correlation of Wave System and Flow Phenomena

Wave generation and identification.- There are two ways to consider pressure waves: The more familiar method is that of an observer in a fixed position who (with waves assumed to be coming from only one direction), upon detecting an increasing (or decreasing) pressure with time, recognizes the arrival of a compression (or expansion) wave. The other method is that of an observer, traveling with the speed of the wave, who (waves again assumed to be coming from only one direction), upon detecting an increasing pressure with time, recognizes the generation of compressions. This moving observer may also determine the type of wave with which he is associated by ascertaining at a given instant of time whether the pressure is lower (or higher) ahead of the wave, in which case he is traveling with a compression (or expansion) wave.

The stationary observer will detect waves only in unsteady flow, whereas the moving observer will detect the growth of waves in a steady flow. As an example of the latter case, consider the pressure drop of a steady flow of air through a friction zone. It may be treated as a system of downstream (P) waves which, although of zero strength before entering the zone, become stronger expansionwise the farther into the zone they traverse. Simultaneously, there is a train of upstream (Q) waves which, also of zero strength initially, grow into stronger compressions as they travel up into the friction zone. These two systems of moving waves combine to form a standing wave, invariant with time, or a pressure drop along the flow. Consequently, a fixed observer would recognize no moving waves in the flow. It might be noted that these trains of waves are the reflections of the waves which produced the steady flow from quiescent air.

Cognizance should also be taken of the fact that the two observers would disagree on the type of supersonic Q waves in a flow. Consider an unsteady compression wave moving upstream against a supersonic flow but actually being washed downstream relative to a fixed coordinate system. The traveling observer looks ahead (upstream), sees lower pressures, and so recognizes a compression wave. The fixed observer, however, first encounters the trailing edge (high pressure) and then at a later instant the leading edge (low pressure) of the wave and apparently recognizes an expansion wave, since the pressure falls with time. Consequently, in supersonic flow the fixed observer must make additional velocity measurements in order to interpret the wave sign correctly.

The unsteady waves generated in the various regions of the shock-tube flow can best be understood by consideration of the following equations which result from equations (1), (2), (3), and differentiation of equation (31)

$$\left.\begin{aligned} &\frac{1}{a_\epsilon}\frac{\delta P}{\delta t} - \frac{1}{\gamma}\frac{a}{a_\epsilon}\frac{\delta \frac{S}{R}}{\delta t} \\ &\frac{1}{a_\epsilon}\frac{\delta Q}{\delta t} - \frac{1}{\gamma}\frac{a}{a_\epsilon}\frac{\delta \frac{S}{R}}{\delta t} \end{aligned}\right\} = \frac{1}{\gamma}\frac{a}{a_\epsilon}\frac{1}{p}\frac{\delta p}{\delta t} \pm \frac{1}{a_\epsilon}\frac{\delta U}{\delta t}$$

$$= \frac{2}{D}\frac{a}{a_\epsilon} U c_f \left\{\left[(\gamma - 1)M \mp 1\right]M + {P_r}^{-2/3}\frac{\theta}{T}\right\} \qquad (60)$$

It is evident that the term $\frac{\delta \frac{S}{R}}{\delta t}$ is not connected with pressure or velocity waves but merely accounts for the change in $\begin{Bmatrix} P \\ Q \end{Bmatrix} = 5a \pm U$ due to traversal of the characteristic through fluid of different entropy. The pressure-wave generation is represented by the change in the difference of these terms and is a result of the skin-friction drag and heat transfer as expressed in the first and second terms, respectively, within the braces on the right-hand side of equation (60).

If equation (60) is now examined from the traveling observer's viewpoint, which is more appropriate since $\frac{\delta(\ )}{\delta t}$ represents the change with time as noticed by the traveling observer, the following facts become obvious:

(1) Upstream (Q) compression waves are generated by the effects of both heat addition to the fluid and skin-friction drag.

(2) Downstream (P) compression waves are generated by heat addition.

(3) Downstream (P) expansion waves are generated by the skin-friction drag if $M < \frac{1}{\gamma - 1}$.

(4) Downstream (P) compression waves are generated by the skin-friction drag if $M > \frac{1}{\gamma - 1}$.

This last result (item (4)) was unexpected since the drag is usually considered as having a braking or decelerating (expansion) effect on the fluid ahead of it.

The following facts might be noted at this point concerning the heat-transfer and skin-friction effects. Expansion waves will be generated in α for shock pressure ratios up to about 5.9 when air at initially uniform temperature throughout is used on both sides of the diaphragm. For pressure ratios above that value, compressions are generated. Also, heat transfer is to the fluid in region α below shock pressure ratios greater than 7.5; above this ratio the adiabatic recovery temperature begins to exceed the wall temperature for $r = 0.9$.

For $M < \frac{1}{\gamma - 1}$ the following conditions then apply for $T_\infty = T_\epsilon = T_{wall}$. In region α heat is being transferred to the fluid. Thus, the effects of heat-transfer and skin-friction drag are additive with regard to the generation of Q compression waves. However, in regard to the generation of P waves, the effects are in opposition since the heat transfer tends to generate compressions and the drag to generate expansions. In region β heat is being lost from the fluid to the walls. The heat transfer and drag are, therefore, cumulative with respect to the production of P expansions and in opposition with respect to Q waves. The stronger waves generated will, consequently, be Q compressions in region α and P expansions in region β, where the drag and heat-transfer effects are cumulative.

Solution for shock pressure ratio of 2.6.- The explanation for the flow behavior may now be considered with these points in mind. The plot of x against t for a shock pressure ratio of 2.6 is shown in figure 13. Adjacent to various points are indicated the values of P', Q', a', U, and p. The primed quantities refer to the values that the parameters would have if an imaginary lamina of fluid with entropy equal to that of the unperturbed flow, but with velocity and pressure identical with the local perturbed flow, were inserted in the flow at these points. In other words, let

$$\frac{1}{a_\epsilon}\frac{\delta P'}{\delta t} = \frac{1}{a_\epsilon}\frac{\delta P}{\delta t} - \frac{1}{\gamma}\frac{a}{a_\epsilon}\frac{\delta \frac{S}{R}}{\delta t} \tag{61}$$

and so on. Then since, by use of the imaginary lamina, the entropy term makes no contribution, P' represents only the pressure and the velocity wave effects.

The reason for the decrease in shock pressure with time is now evident. Just behind the shock the overtaking P expansion waves are growing in strength (P' decreasing) in proportion to the time interval that it takes for the P characteristic to traverse the regions α and β; and, of course, this time interval increases as regions α and β diverge with time.

In figure 13, the values of P' on the β side of the entropy discontinuity are gradually diminishing with time from the value $P'_o = P_{\beta_o} = 6.5451a_\infty$ as weak expansions are generated in region α. These expansions are weak because the skin-friction expansion effect is only slightly stronger than the opposing heat-transfer compression effect. The value of P' slowly decreases with time along the entropy discontinuity as the region α in which the waves are generated becomes larger.

In region β, however, both the skin friction and heat transfer combine to generate strong P' expansions which increase in strength (P' decreasing) rapidly with distance traversed in β. Thus, the first P characteristic shown in figure 13 has experienced a decrement in P' from $P_o = 6.5451$ of only 0.0054 at the entropy discontinuity and of 0.1167 when it overtakes the shock. The second P characteristic shown has a decrement in P' of 0.0105 at the entropy discontinuity and of 0.2032 when it finally overtakes the shock. Note the much greater expansion generated in region β.

The cause of the variation of pressure with time at a given station is not so obvious but may be described in a simple manner for the particular pressure ratio of 2.60 as follows (the explanation is not general since the signs of some of the waves may change with diaphragm pressure ratio): At a given value of x_β, as time increases the incident downstream characteristics have traversed longer distances in α and shorter lengths in β. Now since the drag and heat transfer do not reinforce one another in α, whereas they have an accumulative effect in β on P waves, the effect of decrease in traversal time of β more than offsets the effect of the increase in that of α.

If figure 13 is again used, the following tabulation can be made for the values of the variation in P' along the characteristic for the four characteristics. Subscripts denote regions responsible for the variations.

Characteristics line (fig. 13)	$\delta P'_{\alpha}$ (a)	$\delta P'_{\beta}$	$\Sigma \delta P'$
1	-0.0054	-0.1113	-0.1167
2	-.0105	-.0602	-.0707
3	-.0179	-.0255	-.0434
4	-.0232	-.0047	-.0279

[a]Value includes reflection at entropy discontinuity.

Consequently, even though expansions are being generated in α and β, to a fixed observer at a given x_{β}, the incident downstream waves appear as compressions in that the value of the parameter P' is increasing with time simply because its reduction from the constant value P_{ϵ} is decreasing with time. In other words, the expansion effect generated along the P characteristics up to a given x_{β} is decreasing with time although the net expansion effect up to the shock wave is increasing with time. In addition, the incident Q waves in region β are compression waves (for example, drag effect is larger than heat-transfer effect for this particular case) the strength of which increases with traversal distance (time) from the shock to a fixed x_{β}. The result of these incident waves is thus a pressure rising with time.

The average velocity is increasing with time at a given x_{β} because the "effective compressions," that is $\left(\frac{\partial P'}{\partial t}\right)_x > 0$, downstream are stronger than the upstream compressions. The average velocity of the entropy discontinuity decreases with time because stronger expansions (lower values of P') are overtaking it from behind while simultaneously stronger compressions (higher values of Q') are meeting it from ahead. Both waves are decelerating influences. The average velocity just behind the shock is, of course, decreasing with time and distance. For this particular case, the perfect-fluid velocity is never attained in region β for $t > 0$.

Although the primed quantities of figure 13 give correct values of pressure and averaged velocity, the value of a' is not an indication of the correct average sonic speed since the primed quantities are always evaluated in an imaginary fluid lamina of constant entropy. If the entropy correction were applied, it would be found that the average sonic velocity (temperature) is decreasing with time in region β because the effect of the heat transferred out of the fluid is greater than the combined effect of the compression waves and frictional dissipation. In other words, although the strength of the incident "compression" waves increases with time at a given x, the fluid arriving at that x has been in motion for increasingly longer periods and more energy is lost by heat transfer to the walls, so that the net result is a decrease in temperature.

Assessment of Various Assumptions

The favorable correlation between experiment and linear theory substantiates the use of a small-perturbation approach. However, the limitations of the assumptions used in the analysis must be recognized and weighed carefully before application of the theory to a particular problem.

One of the most precarious assumptions introduced was the averaging process, whereby the quasi-one-dimensional flow was treated as a pure one-dimensional flow in which averaged values of ρ and U were defined as those satisfying the continuity equation integrated over a cross section of the flow. It is known that this assumption will introduce errors in the momentum equation. These errors will be smaller for "full" velocity profiles and, if the boundary-layer profile is assumed not to change with flow travel, will increase in magnitude as the ratio of cross-sectional average velocity to maximum velocity decreases. The errors will also increase as the velocity profile changes shape with flow distance. For example, consider an incompressible steady flow of fluid entering a pipe with a purely one-dimensional rectangular velocity profile which later becomes a parabolic velocity profile some distance along the pipe. The flow has a constant average velocity, yet it requires a pressure drop in excess of that needed to overcome friction to account for the changed velocity profile. Consequently, the averaging process employed in deriving the basic equations may limit the application of the theory to boundary layers which are small relative to tube height and width or which have nearly constant shapes along the tube length.

In addition, if the skin-friction integral is to be evaluated by the use of an equivalent-flat-plate steady flow, there is introduced the assumption of a shock-tube potential flow bounded by a viscous boundary layer. Even without the restrictions of an averaging process, this assumption requires a boundary-layer thickness δ small in relation to the dimensions of the shock-tube width. This restriction was violated in the numerical evaluation of the theory when applied to the experimental results, since the theoretical value of δ at the entropy discontinuity was approximately 1 inch in the $1\frac{1}{2}$- by 2-inch shock tube for $x = 8$ feet for the worst case (shock pressure ratio 1.94). The fact that agreement was still good between theory and experiment even under these conditions indicates that this boundary assumption may be violated markedly without severely penalizing the accuracy of the theory. Of course, when the boundary layer develops to such a degree that it fills the tube and so-called "pipe flow" arises, then the character of the flow will be so altered that a new approach based on pipe flow would probably be more applicable than the boundary-layer and potential-flow approach of the equivalent-flat-plate steady flow.

The assumption of a flow model in which velocity and thermal boundary-layer effects are included by averaging across the channel area is open to further question. This model presumes instantaneous transfer of heat, momentum, and so forth, from the fluid adjacent to the wall to that in the center of the flow. In reality, however, either molecular or macroscopic motion of the particles or transverse pressure waves is necessary for such a transfer so that the influence is felt at the center later than at the walls. Such a delay is usually of second order and can be ignored.

The accuracy of the approximation for the frictional dissipation as equal to the product of wall shearing stress and averaged velocity cannot be verified unless the velocity profile is known; however, this approximation should be good for many cases and is exact for both true one-dimensional flows and Poiseuille flows.

The linearization of the differential equations prevents the application of the theory to large deviations from the theoretical flow. The degree to which this restriction may be stretched is still unknown since the experimental data compared with theory had variations from perfect fluid flow only up to fifteen percent.

In the analysis it was assumed that the leading edge of the expansion wave traveled with a velocity $-a_\epsilon$ and that immediately behind the leading edge the fluid and sonic velocities were U and a_α, respectively. Since the sonic speed varies from a_ϵ to a_α and the fluid velocity from 0 to U as the expansion wave is traversed, the above-mentioned assumption will introduce an error which will magnify as the expansion fan becomes larger at the higher diaphragm pressure ratios. Furthermore, if a more exact treatment were desired for the expansion region, it would be necessary to consider an equivalent accelerating steady flow with a favorable pressure gradient.

In the numerical evaluation of the theory, it was assumed that the functional form of the skin-friction dependency on the flow length ξ was identical for the unsteady flow in the shock tube and the equivalent-flat-plate steady incompressible flow. This assumption has no rigorous argument. Some support may be found in the similarity of the values of c_f obtained from the Rayleigh, Blasius, and modified Blasius solutions. For laminar boundary layers all three solutions give functional relationships, $c_f = (\text{Constant})\sqrt{\frac{\nu}{U\xi}}$, but the constants differ. No comparable solutions are known for turbulent boundary layers. Until some further knowledge is obtained about unsteady boundary layers, it appears that this assumption of the equivalency of steady and unsteady flows must be accepted principally on the basis of agreement between theory and experiment in this range.

When the numerical evaluation of the theory is based on incompressible boundary-layer theory, there is, of course, a source of error as discussed earlier. However, this error can be eliminated by the use of closer compressible boundary-layer approximations in the evaluation of the $c_f(\xi)$ integrals. It should be noted that the effect of the compressibility correction is not as large as might first be expected. Since the Mach number in region β cannot exceed 1.89 for air, although it may go to infinity in region α, the correction to c_f for compressibility will be much larger in α. However, ν_α becomes increasingly less than ν_β as M_α increases, so that the influence of region α decreases. In addition, the compressibility effect will be less on the shock-wave attenuation than on the variation of the flow parameters with time at a given station since the importance of region α on $\delta P'$ changes as discussed in the previous section.

The equivalent-steady-flow model does not give a true picture of the region near the entropy discontinuity even if turbulence is neglected. Since ν is different on each side of the discontinuity, the model yields different boundary-layer thicknesses or an impossible discontinuous boundary layer across the discontinuity. This effect, plus the neglected heat transfer across the entropy discontinuity, apparently is small when examined in the light of the experimental results.

Application of Theory in Shock-Tube Design

The compromise required between aerodynamic and mechanical design of shock tubes for use at high temperatures and Mach numbers becomes evident on scrutiny of the functional form of the equation relating the ratio of the attenuation shock loss or pressure rise (or fall) with time to the ambient pressure. This equation, for c_f proportional to $R_e^{-2/(n+3)}$, is

$$\frac{\Delta p}{p_\infty} = \left[g\left(n, \frac{p_\beta}{p_\infty}\right)\right]\left(\frac{\nu_\infty}{a_\infty D}\right)^{\frac{2}{n+3}}\left(\frac{l}{D}\right)^{\frac{n+1}{n+3}}$$

At a given value of p_β/p_∞, in order to have relatively long flow durations, the ratio l/a_∞ should be large; but insulating problems usually dictate a_∞ in the atmospheric range so that l, consequently, becomes large.

Then in order to minimize the timewise variations at a given x, the ratio l/D should be as small as possible, a requirement prescribing maximum available D. If D is large, mechanical strength of the shock-tube walls will limit the peak shock pressures so that, for large values of p_β/p_∞, it will be necessary to make p_∞ small. A small value of p_∞ will in turn cause ν_∞ to increase so that the reciprocal of the Reynolds number $\nu_\infty/a_\infty D$ rises and with it the attenuation and flow fluctuations. Consequently, the design of the shock tube will be a compromise between mechanical and aerodynamic design, with the l/D term (which has a more powerful exponent than the Reynolds number) probably being the principal aerodynamic consideration.

CONCLUDING REMARKS

Comparison of theoretical and experimental results on the flow in shock tubes appears to substantiate, in the range of the experiments, the method of analysis employed. The application of the basic concepts to much higher pressure ratios and larger perturbations appears logical. However, in such an application, refinement of the linearized procedure may be required to compensate for the crudity of some of the assumptions or it may even be necessary to revert to a step-by-step integration of the basic nonlinear differential characteristic equations and to employ simultaneously skin-friction coefficients based on local velocities. In addition, the basic characteristic equations themselves may require further modification as the shock strength increases to values where dissociation, ionization, and relaxation effects become important. Below the shock strengths where these last-mentioned effects occur, the trends predicted by the linear theory and evaluated in this paper should apply although their magnitude is dependent on the form of skin-friction law assumed.

Although an equivalent steady-flow turbulent boundary-layer solution gave good agreement with the experimental data, application of the theory to cases where the flow Reynolds number is lower than that of these experiments may require the use of laminar boundary-layer solutions. Such lower flow Reynolds numbers would arise either from shocks weaker than those of the experiments advancing into air at atmospheric pressure or from shocks of the same or higher pressure ratio advancing into air below atmospheric pressure. It should also be noted that, at high Reynolds numbers ($> 2 \times 10^7$), the evaluation of the skin-friction coefficient as $0.0581 \times (\text{Reynolds number})^{-1/5}$ becomes inaccurate and should be replaced by a more appropriate relation.

The theoretically predicted trends in the hot gas flow for air at uniform temperature throughout initially are as follows: Shock pressure ratio decreases with distance; static pressure and average values of density, fluid velocity, and Mach number increase with time at a fixed point; and average sonic velocity decreases with time at a fixed point.

Langley Aeronautical Laboratory,
National Advisory Committee for Aeronautics,
Langley Field, Va., December 7, 1954.

APPENDIX A

DERIVATION OF CHARACTERISTIC EQUATIONS FOR QUASI-ONE-DIMENSIONAL CHANNEL FLOW WITH AREA CHANGE, FRICTION, AND HEAT ADDITION

The general form of the quasi-one-dimensional continuity equation is expressed as

$$\frac{\partial}{\partial t}(\rho A) + \frac{\partial}{\partial x}(\rho UA) = 0 \tag{A1}$$

$$\frac{\partial \log_e A}{\partial t} + U \frac{\partial \log_e A}{\partial x} + \frac{\partial \log_e \rho}{\partial t} + U \frac{\partial \log_e \rho}{\partial x} + \frac{\partial U}{\partial x} = 0 \tag{A2}$$

If averaged values across a section of the flow are employed for ρ and U when channel flows are considered, the area term A represents only the physical cross-sectional area and boundary-layer displacement thickness is of no concern.

The identities

$$a^2 \equiv \gamma RT \tag{A3}$$

and

$$d \frac{S}{R} \equiv \frac{d(\text{Heat added})}{RT} \tag{A4}$$

combined with the equations of state and energy yield the following familiar relationships:

$$\rho = (\text{Constant})\ a^{2c_v/R}\ e^{-S/R} \tag{A5}$$

$$p = (\text{Constant})\ a^{2c_p/R}\ e^{-S/R} \tag{A6}$$

Now, if all the fluid under consideration has been in the same state at any previous time, equations (A5) and (A6) may be differentiated with respect to x and t with no contribution from the constant term.

$$\frac{\partial \log_e \rho}{\partial x} = \frac{2c_v}{R}\frac{\partial \log_e a}{\partial x} - \frac{\partial \frac{S}{R}}{\partial x} \tag{A7a}$$

$$\frac{\partial \log_e \rho}{\partial t} = \frac{2c_v}{R}\frac{\partial \log_e a}{\partial t} - \frac{\partial \frac{S}{R}}{\partial t} \tag{A7b}$$

$$\frac{\partial \log_e p}{\partial x} = \frac{2c_p}{R}\frac{\partial \log_e a}{\partial x} - \frac{\partial \frac{S}{R}}{\partial x} \tag{A7c}$$

$$\frac{\partial \log_e p}{\partial t} = \frac{2c_p}{R}\frac{\partial \log_e a}{\partial t} - \frac{\partial \frac{S}{R}}{\partial t} \tag{A7d}$$

The momentum equation is then written by use of the skin-friction coefficient and hydraulic diameter as

$$\frac{\partial U}{\partial t} + U\frac{\partial U}{\partial x} + \frac{1}{\rho}\frac{\partial p}{\partial x} + \frac{2U^2c_f}{D} = 0 \tag{A8}$$

This equation is not exact, since the effective values of ρ and U were chosen to satisfy the continuity equation; however, for "full" velocity profiles (that is, profiles in which the velocity deviates only slightly from its maximum value in a large part of the cross section), equation (A8) is a good approximation.

Equations (A8) and (A2) can be rearranged, after substituting from equation (A7) and employing the convective derivative

$$\frac{D(\ )}{Dt} = \frac{\partial(\ )}{\partial t} + U\frac{\partial(\ )}{\partial x} \tag{A9}$$

to give

$$\frac{DU}{Dt} + \frac{2c_v}{R} a \frac{\partial a}{\partial x} - \frac{a^2}{\gamma} \frac{\partial \frac{S}{R}}{\partial x} + \frac{2U^2 c_f}{D} = 0 \tag{A10}$$

$$\frac{2c_v}{R} \frac{Da}{Dt} + a \frac{\partial U}{\partial x} - a \frac{D \frac{S}{R}}{Dt} + a \frac{D \log_e A}{Dt} = 0 \tag{A11}$$

Equations (A10) and (A11) may be added and subtracted to give the following equations in operator form:

$$\left(\frac{D}{Dt} + a \frac{\partial}{\partial x}\right)\left(\frac{2c_v}{R} a + U\right) = -a \frac{D \log_e A}{Dt} + \frac{a}{\gamma}\left(\frac{D}{Dt} + a \frac{\partial}{\partial x}\right)\frac{S}{R} + \frac{\gamma - 1}{\gamma} a \frac{D \frac{S}{R}}{Dt} - \frac{2U^2 c_f}{D} \tag{A12}$$

$$\left(\frac{D}{Dt} - a \frac{\partial}{\partial x}\right)\left(\frac{2c_v}{R} a - U\right) = -a \frac{D \log_e A}{Dt} + \frac{a}{\gamma}\left(\frac{D}{Dt} - a \frac{\partial}{\partial x}\right)\frac{S}{R} + \frac{\gamma - 1}{\gamma} a \frac{D \frac{S}{R}}{Dt} + \frac{2U^2 c_f}{D} \tag{A13}$$

The assumption has been made in equations (A12) and (A13) that c_v/R is constant. Now, from the definition of the derivative along a characteristic of slope $\delta x/\delta t$ equal to $U \pm a$ as

$$\frac{\delta(\ )}{\delta t} = \frac{\partial(\ )}{\partial t} + (U \pm a)\frac{\partial(\ )}{\partial x} = \frac{D(\ )}{Dt} \pm a \frac{\partial(\ )}{\partial x} \tag{A14}$$

equations (A12) and (A13) may be written in the final form:

$$\frac{\delta P}{\delta t} = \frac{\delta}{\delta t}\left(\frac{2c_v}{R} a + U\right) = -a \frac{D \log_e A}{Dt} + \frac{a}{\gamma} \frac{\delta \frac{S}{R}}{\delta t} + \frac{\gamma - 1}{\gamma} a \frac{D \frac{S}{R}}{Dt} - \frac{2U^2 c_f}{D} \tag{A15}$$

$$\frac{\delta Q}{\delta t} = \frac{\delta}{\delta t}\left(\frac{2c_v}{R} a - U\right) = -a \frac{D \log_e A}{Dt} + \frac{a}{\gamma} \frac{\delta \frac{S}{R}}{\delta t} + \frac{\gamma - 1}{\gamma} a \frac{D \frac{S}{R}}{Dt} + \frac{2U^2 c_f}{D} \tag{A16}$$

APPENDIX B

EVALUATION OF CONVECTIVE DERIVATIVE OF ENTROPY

The convective derivative of entropy may be expressed in the form

$$\frac{D\frac{S}{R}}{Dt} = \frac{1}{RT}\left(\frac{DJ}{Dt} + \frac{DH_f}{Dt}\right) \tag{B1}$$

where DJ/Dt represents the heat added per unit mass by heat transfer and heat sources while DH_f/Dt represents the heat dissipated per unit mass by friction.

The heat transfer per unit mass from the walls may be approximated as $4h\theta/\rho D$ where θ is the difference between the wall temperature and the recovery temperature of the flow; for example,

$$\theta = T_{wall} - T_{flow}\left(1 + r\,\frac{\gamma - 1}{2}\,M^2\right) \tag{B2}$$

The assumption is next introduced that the relation between heat transfer and skin friction is given by a modified form of Reynolds' analogy which is assumed to apply for turbulent as well as for laminar boundary layers in both steady and unsteady flow. Substitution of the perfect gas law into the modified form of Reynolds' analogy results in the following equation for the wall heat-transfer coefficient:

$$h = \frac{1}{2}\,\frac{\gamma}{\gamma - 1}\,R\rho U {P_r}^{-2/3} c_f \tag{B3}$$

The heat-transfer term may then be written as

$$\frac{DJ}{Dt} = \frac{2\gamma}{\gamma - 1}\,\frac{R\theta}{D}\,U c_f {P_r}^{-2/3} \tag{B4}$$

The frictional dissipation per unit mass is assumed to be the product of the average velocity multiplied by the wall-shearing force and divided by the mass in the flow:

$$\frac{DH_f}{Dt} = \frac{U\tau(\text{Perimeter})\Delta x}{\rho A\ \Delta x} = \frac{2U^3}{D} c_f \tag{B5}$$

Although equation (B5) is not exact in general, it is a good approximation for most cases. It might be noted that equation (B5) is exact for a true one-dimensional-flow model where the velocity is considered constant across a cross section of the flow with a discontinuity in velocity at the wall. It is also exact for incompressible Poiseuille flow since the dissipation function, $\int \mu\left(\frac{\partial u}{\partial y}\right)^2 dy$, reduces to the value of equation (B5).

Therefore, under the conditions presumed to apply above, equations (B1), (B4), and (B5) may be combined to evaluate the convective derivative

$$\frac{D\frac{S}{R}}{Dt} = \left(M^2 + \frac{1}{\gamma - 1}\frac{\theta}{T} P_r^{-2/3}\right)\frac{2\gamma}{D} Uc_f \tag{B6}$$

APPENDIX C

LINEARIZED SOLUTION FOR INTERSECTION OF CHARACTERISTICS AND ENTROPY DISCONTINUITY

The linearized solution for the intersection of the characteristic lines with an entropy discontinuity is obtained in the following manner (see fig. 1 for notation):

$$\delta P \equiv P_f - P_c = Q_f - Q_c = \frac{2}{\gamma - 1} a_c\left(\frac{a_f}{a_c} - 1\right) \tag{C1}$$

$$P_c + Q_f = \frac{2}{\gamma - 1} a_c\left(\frac{a_f}{a_c} + 1\right) \tag{C2}$$

In these equations the values of γ are assumed to be identical everywhere.

Dividing equation (C1) by (C2) and applying the condition that the pressures are always equal to one another at any instant on both sides of the discontinuity yields

$$\frac{\delta P}{P_c + Q_f} = \frac{e^{\frac{S_f - S_c}{2c_p}} - 1}{e^{\frac{S_f - S_c}{2c_p}} + 1} \tag{C3}$$

Now, if the subscript o denotes conditions at time $t = 0$ immediately after the diaphragm burst with

$$\Delta S \equiv S_f - S_c \tag{C4}$$

or

$$\Delta S = \Delta S_o(1 + \lambda) \quad \text{where} \quad \lambda \ll 1 \tag{C5}$$

and

$$\frac{a_{\beta_o}}{a_{\alpha_o}} = e^{\frac{\Delta S_o}{2c_p}} \tag{C6}$$

substituting equation (C5) in equation (C3) and expanding gives

$$\frac{\delta P}{P_c + Q_f} = \left(\frac{e^{\frac{\Delta S_o}{2c_p}} - 1}{e^{\frac{\Delta S_o}{2c_p}} + 1}\right)\left(1 + 2\lambda \frac{\Delta S_o}{2c_p} \frac{e^{\frac{\Delta S_o}{2c_p}}}{e^{\frac{\Delta S_o}{c_p}} - 1} + \cdot\ \cdot\ \cdot\ \cdot\ \cdot\right) \tag{C7}$$

or

$$\frac{\delta P}{\delta P_o} = \frac{P_c + Q_f}{P_{\alpha_o} + Q_{\beta_o}}\left[1 + \lambda \frac{\Delta S_o}{c_p} \frac{a_{\beta_o}/a_{\alpha_o}}{\left(\frac{a_{\beta_o}}{a_{\alpha_o}}\right)^2 - 1} + \cdot\ \cdot\ \cdot\ \cdot\ \cdot\right] \tag{C8}$$

$$\frac{\delta P}{\delta P_o} = \left[1 + \frac{\left(P_c - P_{\alpha_o}\right) + \left(Q_f - Q_{\beta_o}\right)}{P_{\alpha_o} + Q_{\beta_o}}\right]\left[1 + \lambda \frac{\Delta S_o}{c_p} \frac{a_{\beta_o}/a_{\alpha_o}}{\left(\frac{a_{\beta_o}}{a_{\alpha_o}}\right)^2 - 1} + \cdot\ \cdot\ \cdot\ \cdot\ \cdot\right] \tag{C9}$$

Since $\dfrac{P_c - P_{\alpha_o}}{P_{\alpha_o} + Q_{\beta_o}}$ and $\dfrac{Q_f - Q_{\beta_o}}{P_{\alpha_o} + Q_{\beta_o}}$ are of order λ, the first-order or linearized solution becomes

$$\frac{\delta P}{\delta P_o} = \frac{\delta Q}{\delta Q_o} = 1 + \frac{\left(P_c - P_{\alpha_o}\right) + \left(Q_f - Q_{\beta_o}\right)}{P_{\alpha_o} + Q_{\beta_o}} +$$

$$\frac{\gamma - 1}{\gamma} \frac{a_{\beta_o}/a_{\alpha_o}}{\left(\dfrac{a_{\beta_o}}{a_{\alpha_o}}\right)^2 - 1} \left(\frac{S_f - S_{\beta_o}}{R} - \frac{S_c - S_{\alpha_o}}{R}\right) \tag{C10}$$

APPENDIX D

RELATION BETWEEN SKIN-FRICTION COEFFICIENT AND VELOCITY PROFILE

The relation between skin-friction coefficient and velocity profile for an incompressible turbulent boundary layer on a flat plate may be found in the following manner. Let the velocity profile in the boundary layer be of the form $\frac{u_y}{U} = \left(\frac{y}{\delta}\right)^{1/n}$ where u_y is the local streamwise velocity at the distance y from the plate and δ is the boundary-layer thickness. Then, equating the wall shearing stress τ to the rate of decrease, in the streamwise ξ direction, of the momentum in the boundary layer gives

$$\tau = \frac{d}{d\xi}\int_0^\delta \rho u_y(U - u_y)dy \tag{D1}$$

Evaluation of this equation for constant ρ yields

$$\frac{\tau}{\rho U^2} = \frac{n}{(n + 1)(n + 2)}\frac{d\delta}{d\xi} + \frac{(2 - n^2)\delta}{(n + 1)^2(n + 2)^2}\frac{dn}{d\xi} \tag{D2}$$

The following relations are then assumed between the shearing-stress velocity U^* and the boundary-layer thickness δ (see ref. 10):

$$U^{*2} \equiv \frac{\tau}{\rho} \tag{D3}$$

$$\frac{U}{U^*} = B\left(\frac{U^*\delta}{\nu}\right)^{1/n} \tag{D4}$$

The parameter B may be assumed a constant for n invariant with ξ, but its form for $n = n(\xi)$ is not specified.

Substitution of equations (D3) and (D4) into equation (D2) results in the following differential equation:

$$\delta^{\frac{2}{n+1}} \frac{d\delta}{d\xi} = \frac{1}{U^2}\left(\frac{U\nu^{1/n}}{B}\right)^{\frac{2n}{n+1}} \frac{(n + 1)(n + 2)}{n} - \frac{(2 - n^2)}{n(n + 1)(n + 2)} \delta^{\frac{n+3}{n+1}} \frac{dn}{d\xi} \tag{D5}$$

For the case of n and B independent of ξ, equation (D5) may be integrated, by assuming $n \neq -1$. This integration with application of the boundary condition of $\delta = 0$ at $\xi = 0$ produces

$$\delta = \frac{\nu}{UB^n}\left[\frac{(n + 2)(n + 3)}{n} B^n \frac{U}{\nu}\right]^{\frac{n+1}{n+3}} \xi^{\frac{n+1}{n+3}} \tag{D6}$$

Substitution of equation (D6) into equation (D2) results in the expression for the skin-friction coefficient:

$$c_f(\xi) = \frac{\tau(\xi)}{\rho U^2/2} = 2\left[\frac{n}{(n + 2)(n + 3)B^n}\right]^{\frac{2}{n+3}} \left(\frac{\nu}{U\xi}\right)^{\frac{2}{n+3}} \tag{D7}$$

REFERENCES

1. Lobb, R. K.: A Study of Supersonic Flows in a Shock Tube. UTIA Rep. No. 8, Inst. of Aerophysics, Univ. of Toronto, May 1950.

2. Huber, Paul W., Fitton, Cliff E., Jr., and Delpino, F.: Experimental Investigation of Moving Pressure Disturbances and Shock Waves and Correlation With One-Dimensional Unsteady-Flow Theory. NACA TN 1903, 1949.

3. Hollyer, Robert N., Jr.: A Study of Attenuation in the Shock Tube. Proj. M720-4 (Contract N6-ONR-232-TO IV, Off. of Naval Res.), Univ. of Michigan Eng. Res. Inst., July 1, 1953.

4. Geiger, F. W. and Mautz, C. W.: The Shock Tube as an Instrument for the Investigation of Transonic and Supersonic Flow Patterns. Proj. M720-4 (Contract N6-ONR-232, Navy Res. Project), Univ. of Michigan Eng. Res. Inst., June 1949. (With Addendum by R. N. Hollyer, Jr.)

5. Emrich, R. J., and Curtis, C. W.: Attenuation in the Shock Tube. Jour. of Appl. Phys., vol. 24., no. 3, Mar. 1953, pp. 360-363.

6. Donaldson, Coleman duP., and Sullivan, Roger D.: The Effect of Wall Friction on the Strength of Shock Waves in Tubes and Hydraulic Jumps in Channels. NACA TN 1942, 1949.

7. Glass, I. I., Martin, W., and Patterson, G. N.: A Theoretical and Experimental Study of the Shock Tube. UTIA Rep. No. 2, Inst. of Aerophysics, Univ. of Toronto, Nov. 1953.

8. Mack, John E.: Density Measurement in Shock Tube Flow With the Chrono-Interferometer. Tech. Rep. 4, Lehigh Univ. Inst. of Res. (Proj. NR-061-063, Contract N7-ONR-39302, Off. of Naval Res.), Apr. 15, 1954.

9. Schlichting, H.: Lecture Series "Boundary Layer Theory." Part I - Laminar Flows. NACA TM 1217, 1949.

10. Schlichting, H.: Lecture Series "Boundary Layer Theory." Part II - Turbulent Flows. NACA TM 1218, 1949.

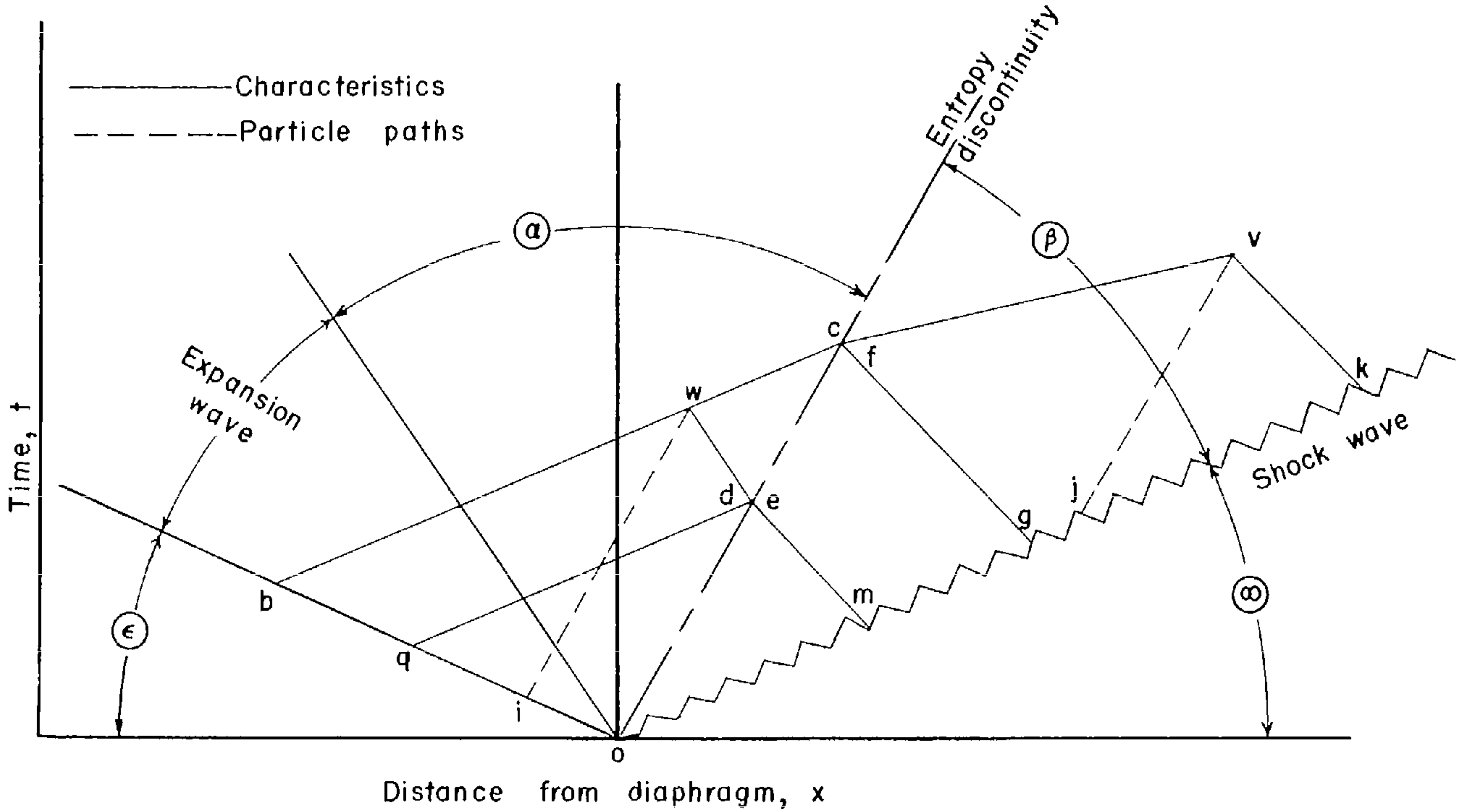
Characteristics
Particle paths
Entropy discontinuity
α
β
Expansion wave
Shock wave
ϵ
∞
v
c
f
k
w
d
e
j
g
b
m
q
i
o
Time, t
Distance from diaphragm, x

Figure 1.- Distance-time plot of shock-tube flow.

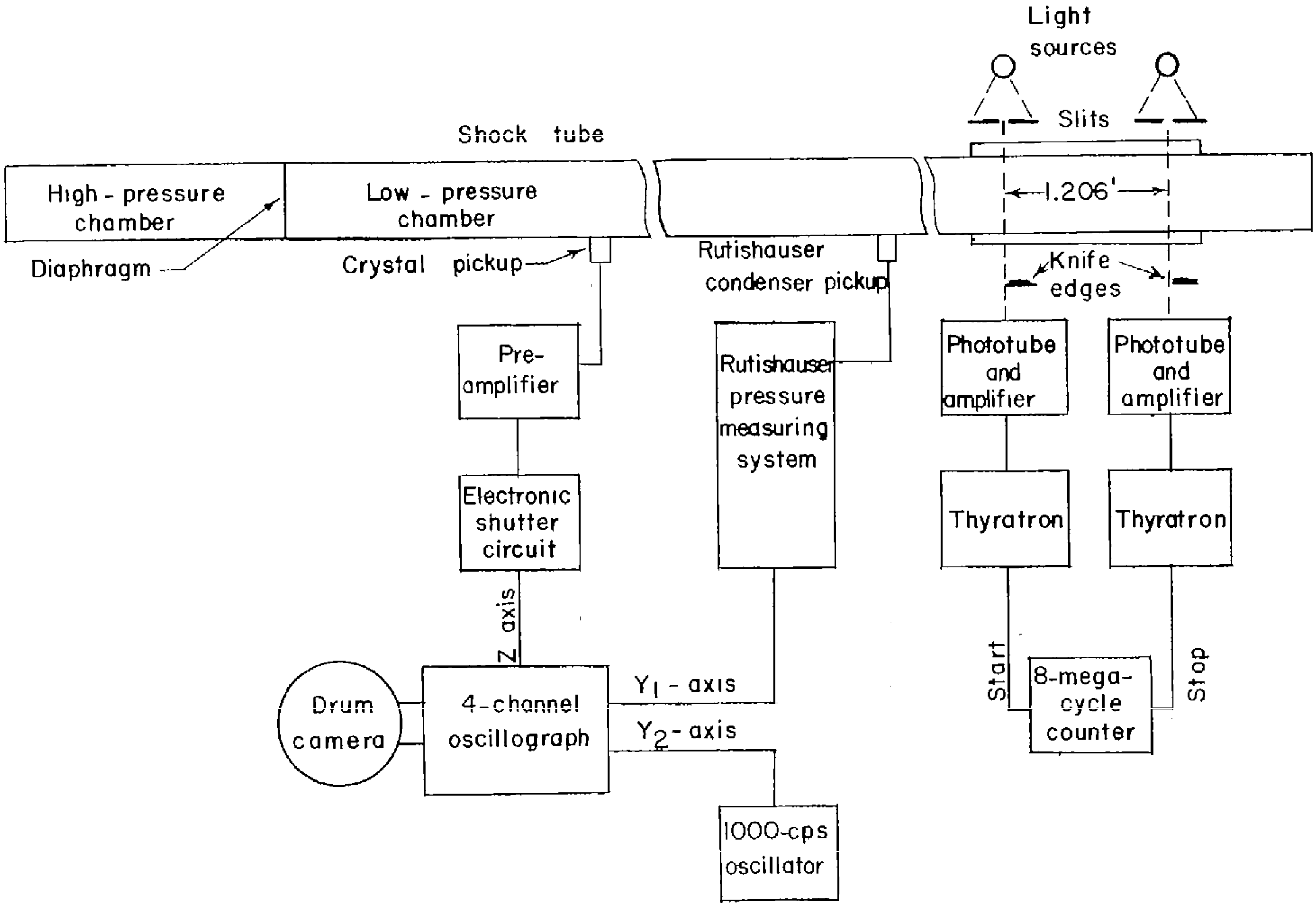
Light sources
Slits
Shock tube
High - pressure chamber
Low - pressure chamber
Diaphragm
Crystal pickup
Rutishauser condenser pickup
1.206'
Knife edges
Pre-amplifier
Rutishauser pressure measuring system
Phototube and amplifier
Phototube and amplifier
Electronic shutter circuit
Thyratron
Thyratron
Z axis
Start
Stop
8-mega-cycle counter
Drum camera
4-channel oscillograph
Y_1 - axis
Y_2 - axis
1000-cps oscillator

Figure 2.- Schematic diagram of test equipment. (All power voltage regulated at 115 volts, alternating current.)

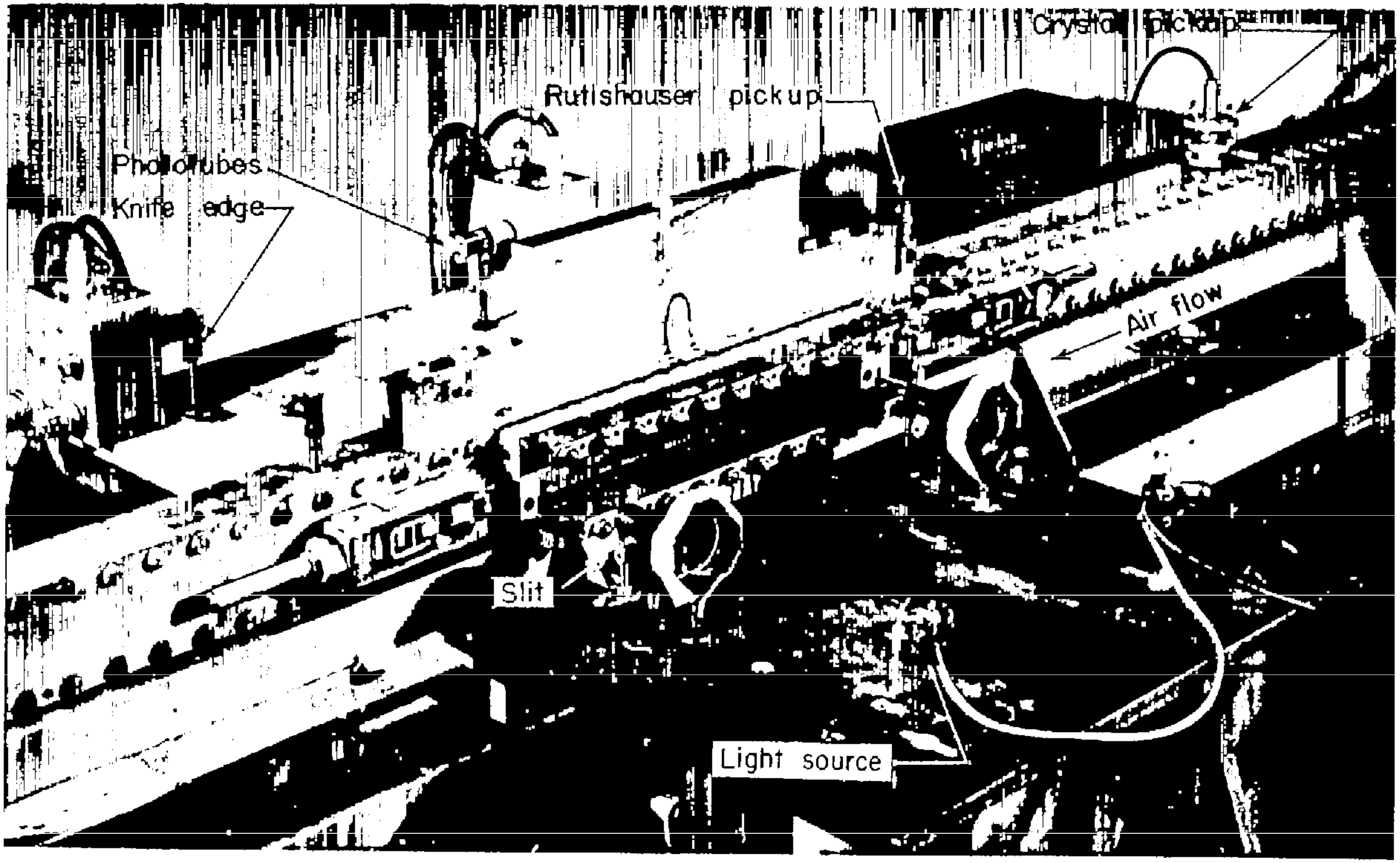
Crystal pickup
Rutishauser pickup
Phototubes
Knife edge
Air flow
Slit
Light source

L-85316.1

Figure 3.- Photograph of measuring station in shock tubes.

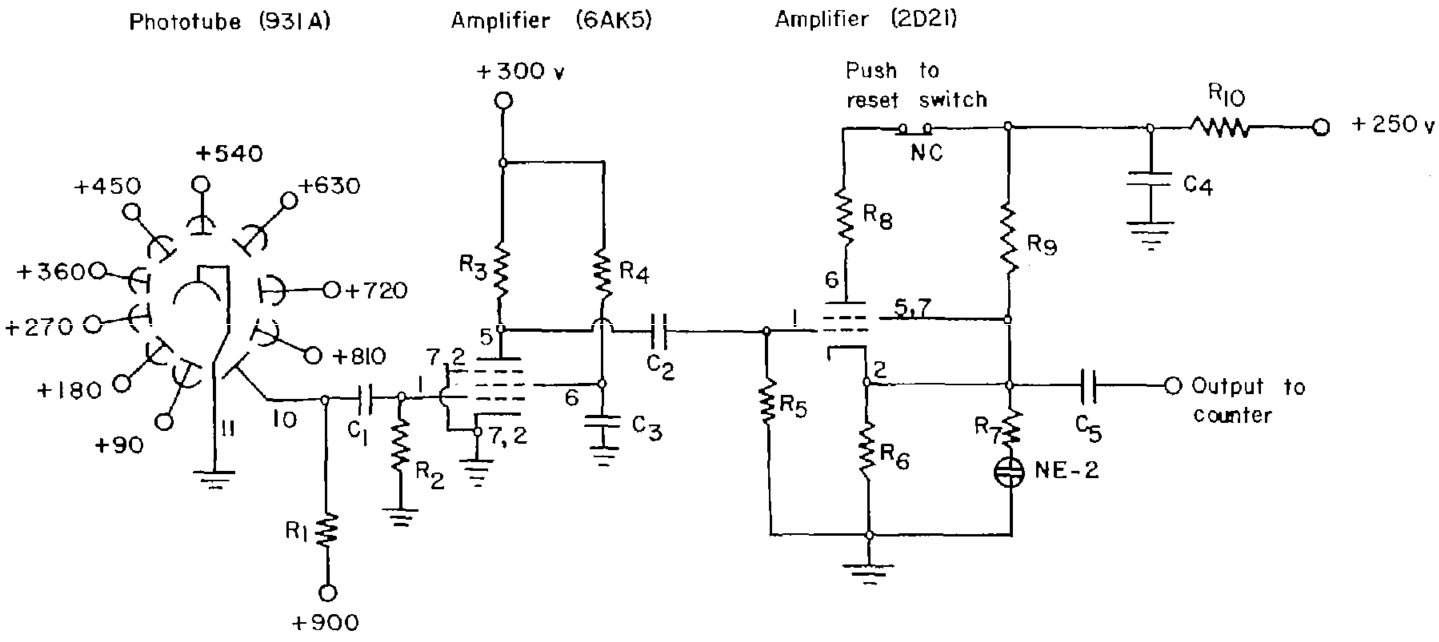
Phototube (931A)
Amplifier (6AK5)
Amplifier (2D21)
+300 v
Push to reset switch
NC
R10
+250 v
C4
R8
R9
6
5,7
1
2
R3
R4
5
7,2
1
7,2
6
C2
C3
R5
R6
R7
C5
NE-2
Output to counter
+540
+450
+630
+360
+720
+270
+810
+180
+90
11
10
C1
R2
R1
+900

Dynode
Anode
Photocathode

R_1	22K	R_6	22K 2w	C_1	300 $\mu\mu$fd		
R_2	22K	R_7	470K 1/2w	C_2	300 $\mu\mu$fd		
R_3	22 K	R_8	15 K 2 w	C_3	0.001 μfd		
R_4	100 K	R_9	1.2 megohm 1/2 w	C_4	16 μfd 450 v		
R_5	100 K 1/2 w	R_{10}	3.3 K 2 w	C_5	0.001 μfd 600 v		

Figure 4.- Circuit diagram of phototube and amplifiers.

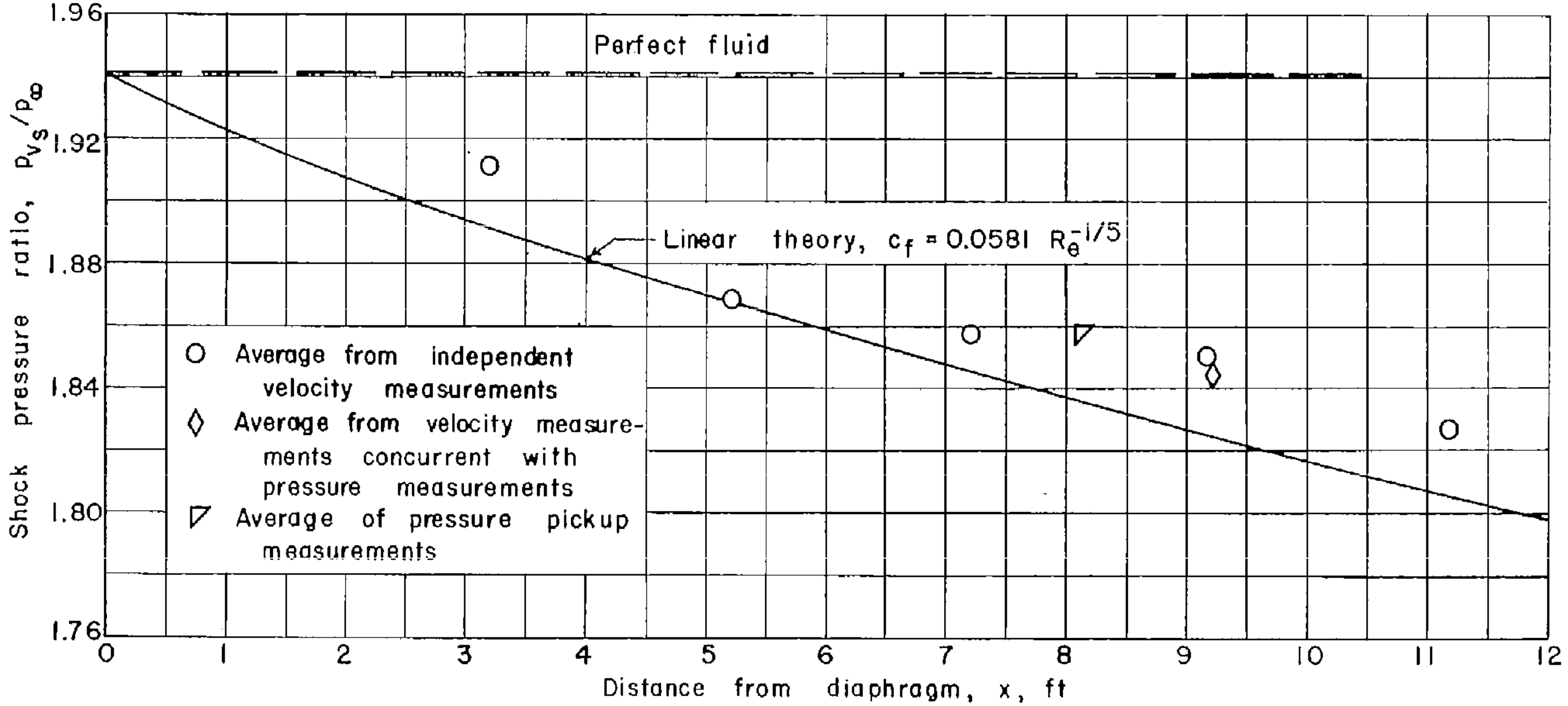

(a) p_ϵ = 45 lb/sq in. gage. Experimental data corrected to p_ϵ/p_∞ = 4.061.

Figure 5.- Theoretical and experimental shock pressure ratio plotted against distance from diaphragm.

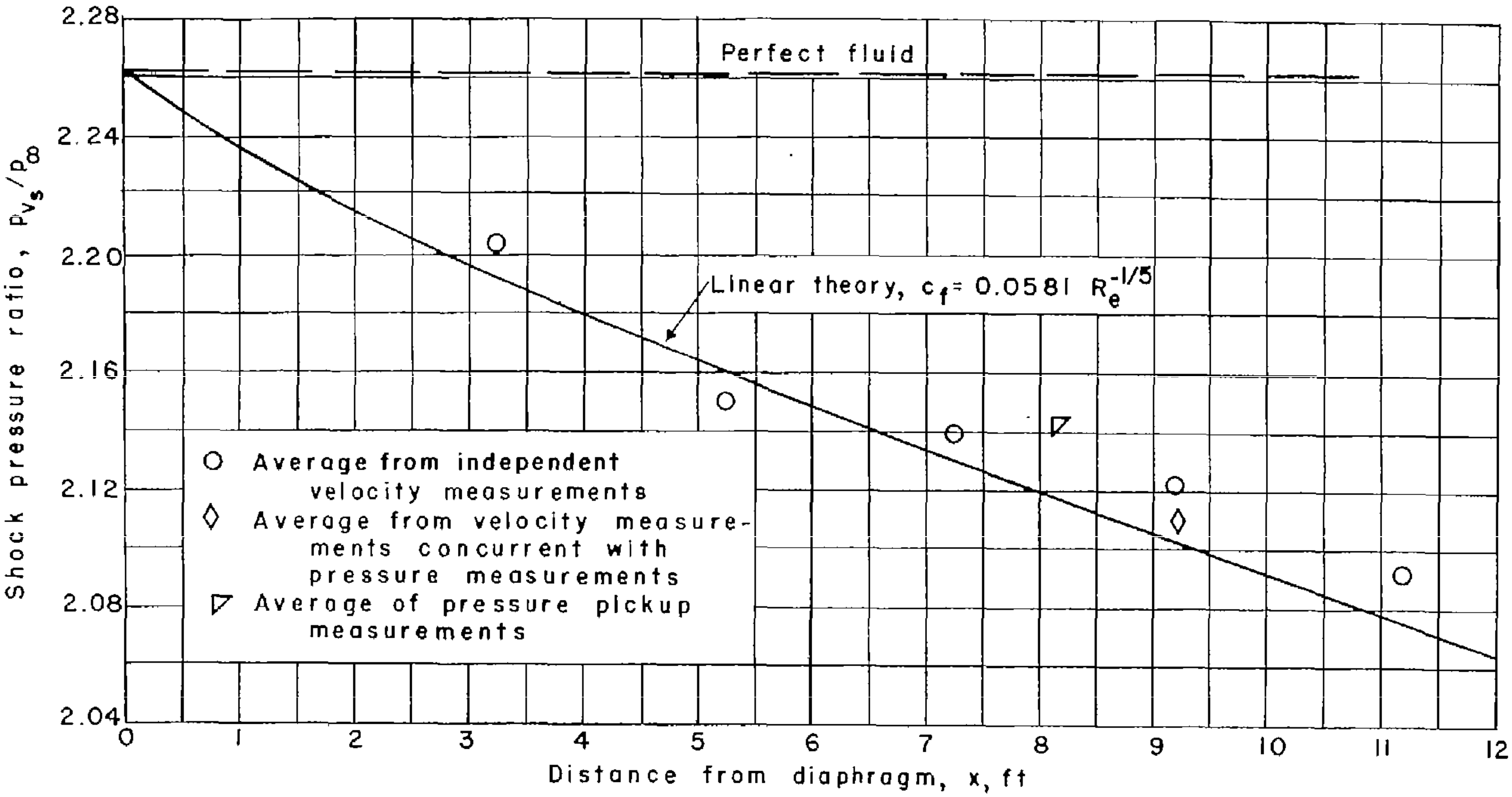

(b) p_ϵ = 70 lb/sq in. gage. Experimental data corrected to $p_\epsilon/p_\infty = 5.764$.

Figure 5.- Continued.

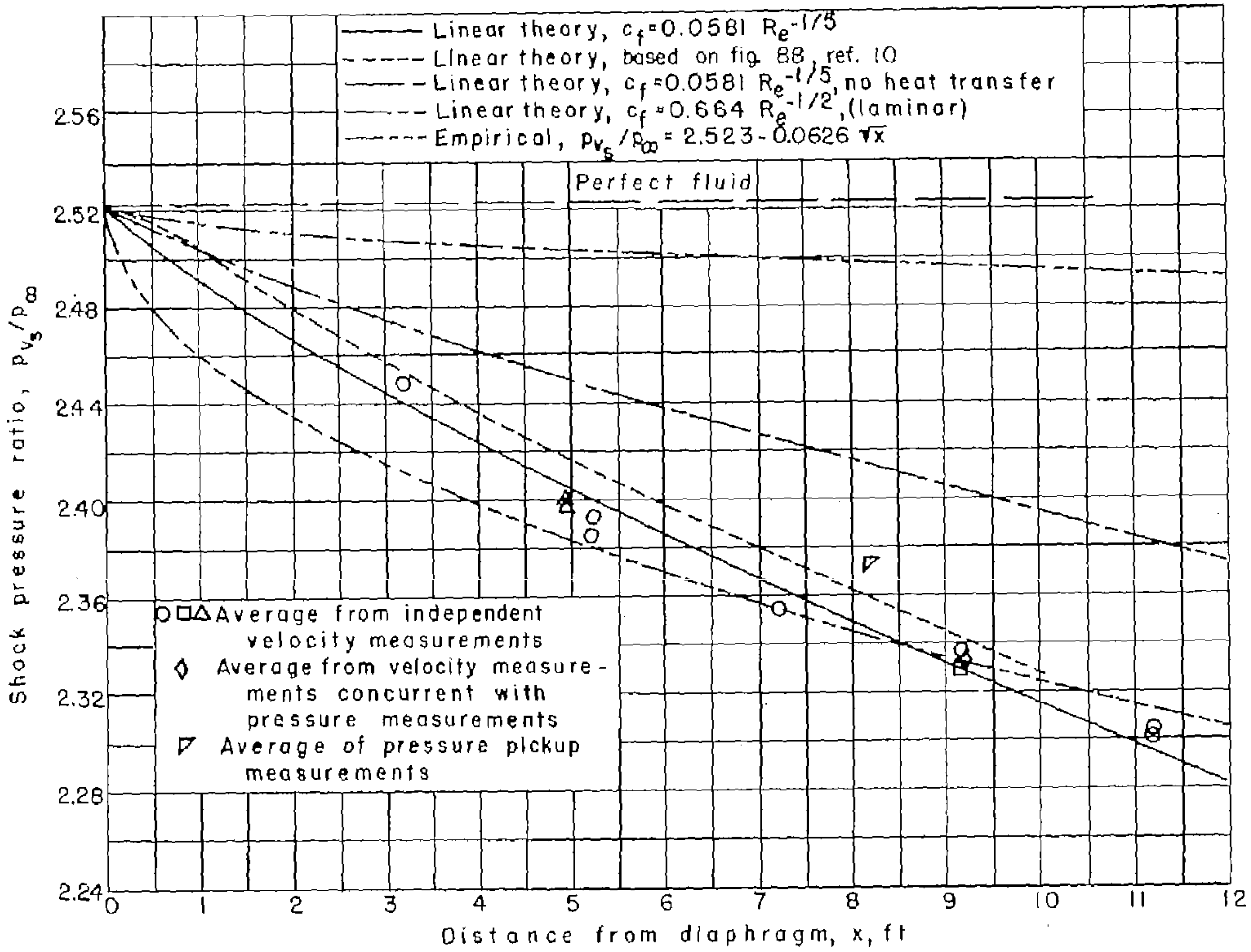

(c) p_ϵ = 95 lb/sq in. gage. Experimental data corrected to $p_\epsilon/p_\infty = 7.455$.

Figure 5.- Continued.

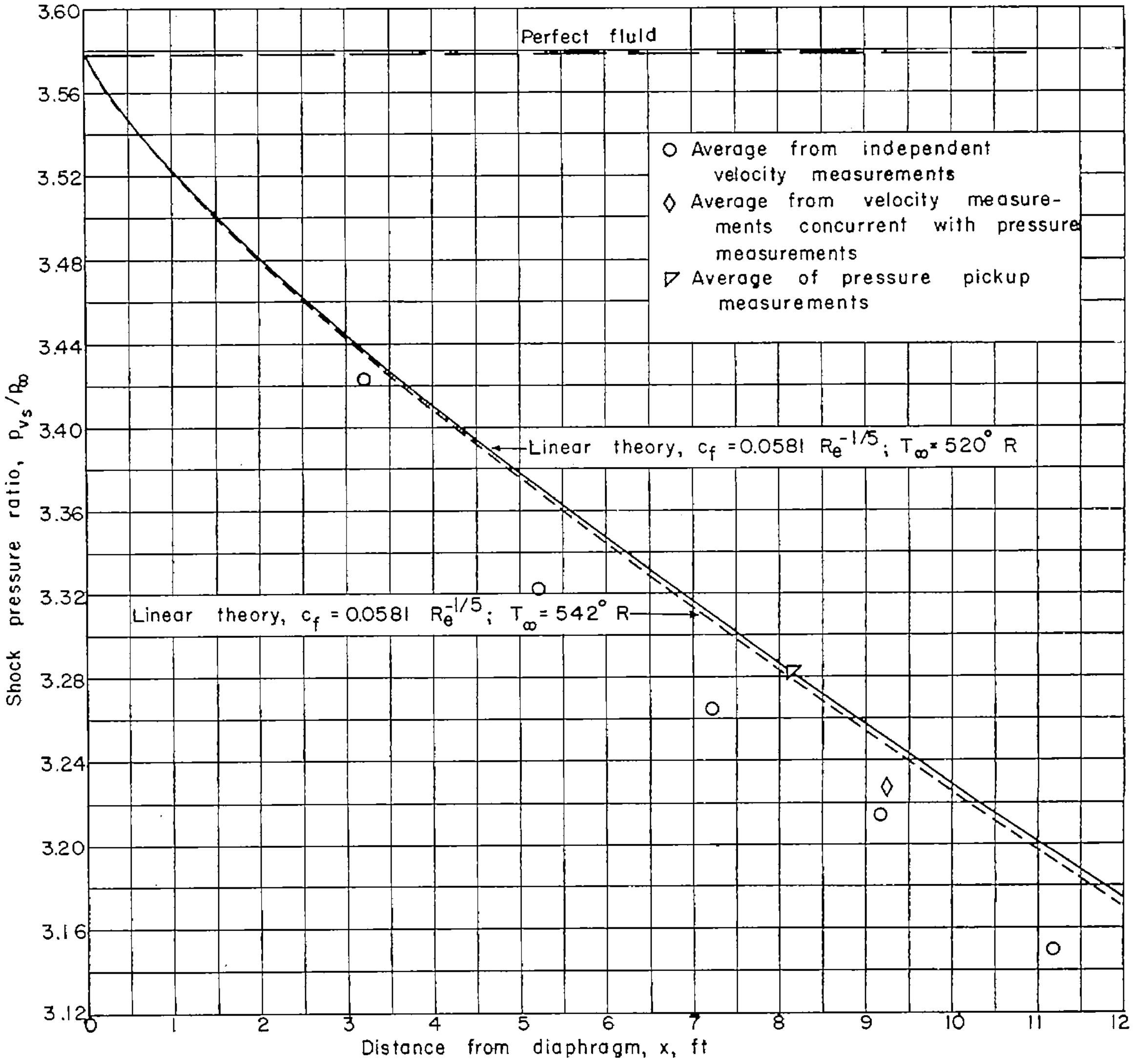

(d) p_ϵ = 250 lb/sq in. gage. Experimental data corrected to p_ϵ/p_∞ = 17.915.

Figure 5.- Concluded.

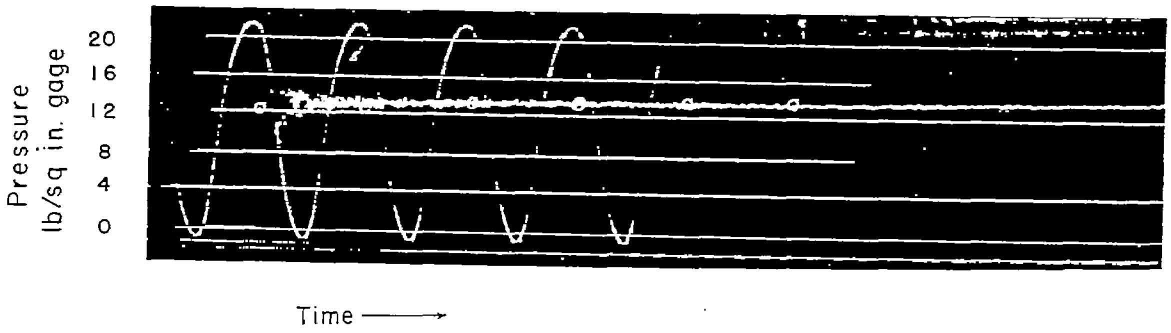

(a) $p_\epsilon/p_\infty = 4.061$.

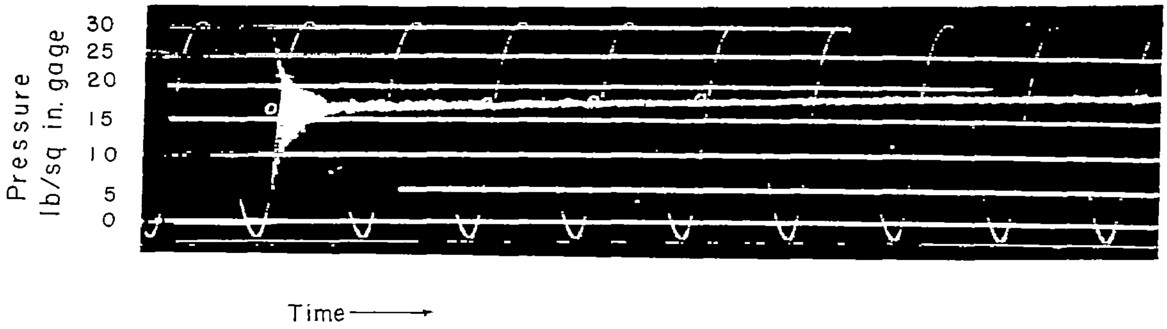

(b) $p_\epsilon/p_\infty = 5.764$.

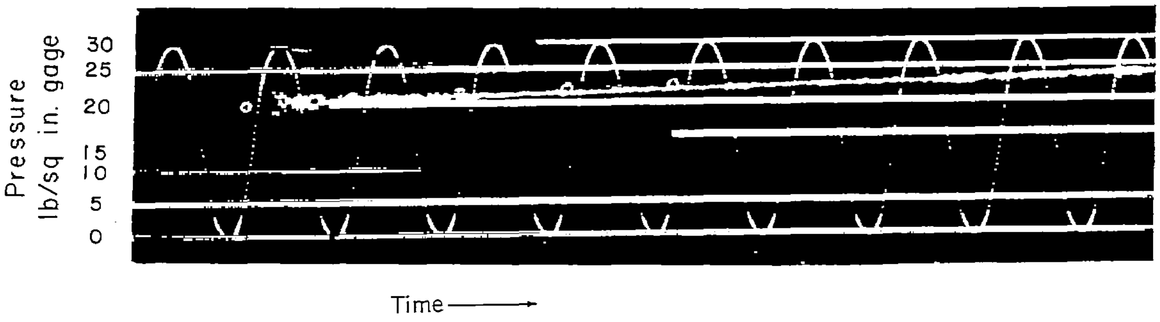

(c) $p_\epsilon/p_\infty = 7.455$.

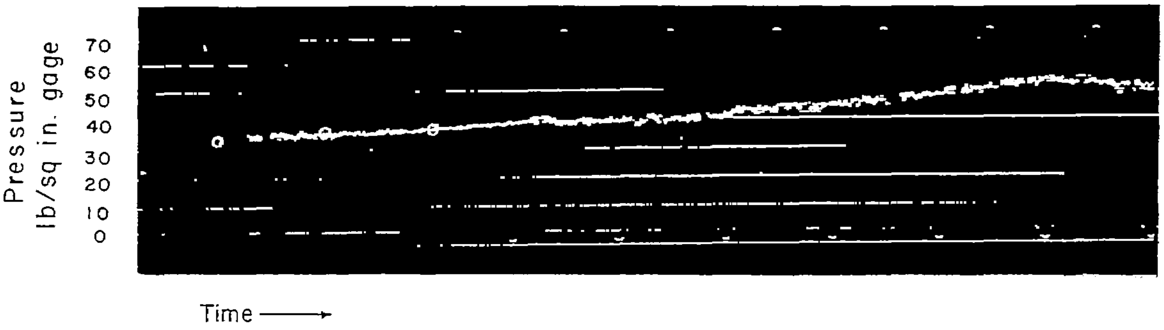

(d) $p_\epsilon/p_\infty = 17.915$.

Figure 6.- Comparison of experimental and theoretical pressure-time curves. $x_{exp} = 8.13$ feet; $x_{theor} = 8.0$ feet. Circles represent theoretical values. The sine-wave time base has a frequency of 1,000 cps.

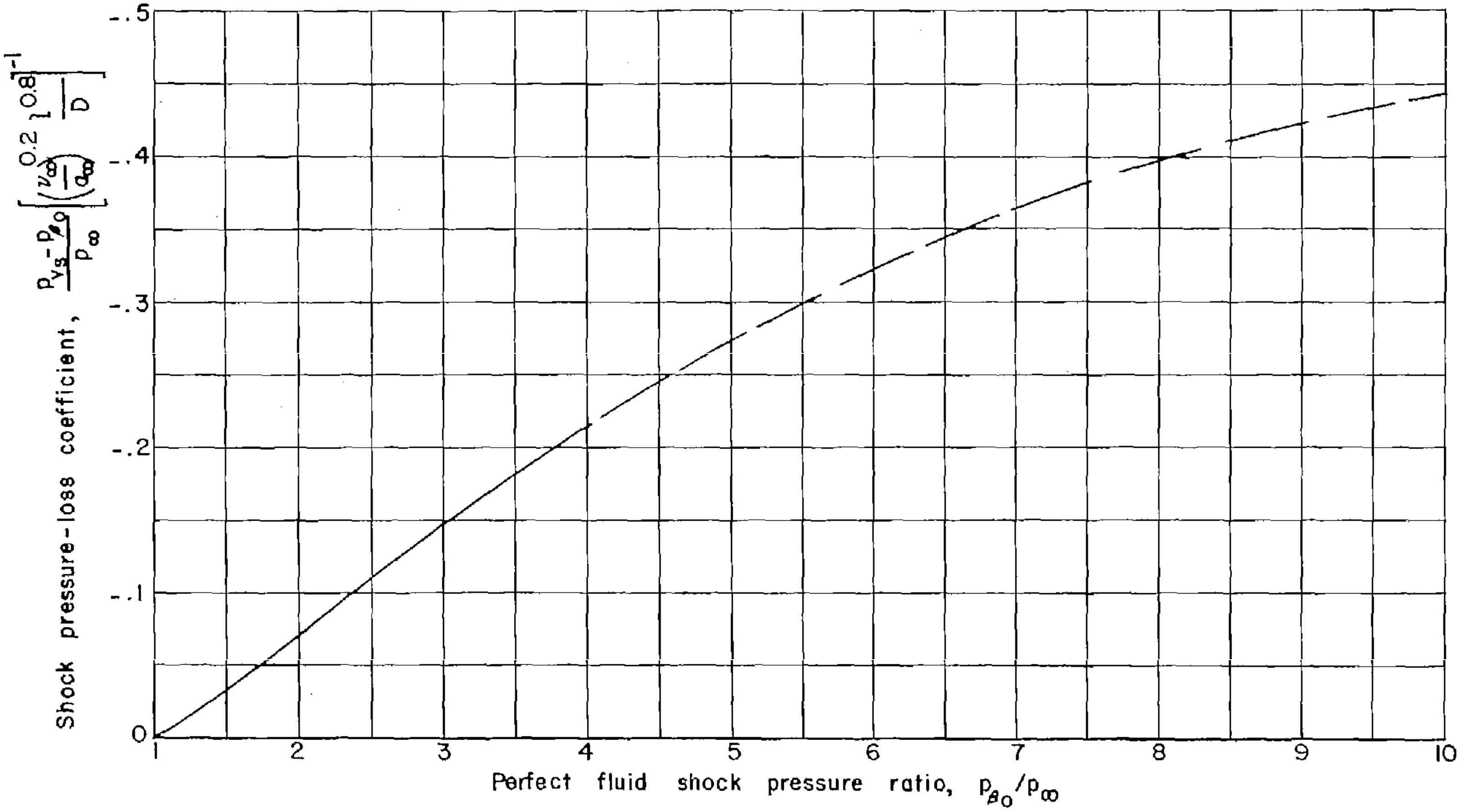

(a) Shock pressure-loss coefficient.

Figure 7.- Variation of shock pressure-loss and shock pressure-attenuation coefficients with perfect-fluid shock pressure ratio. $a_\epsilon = a_\infty$; $n = 7$; $c_f = 0.0581R_e^{-1/5}$.

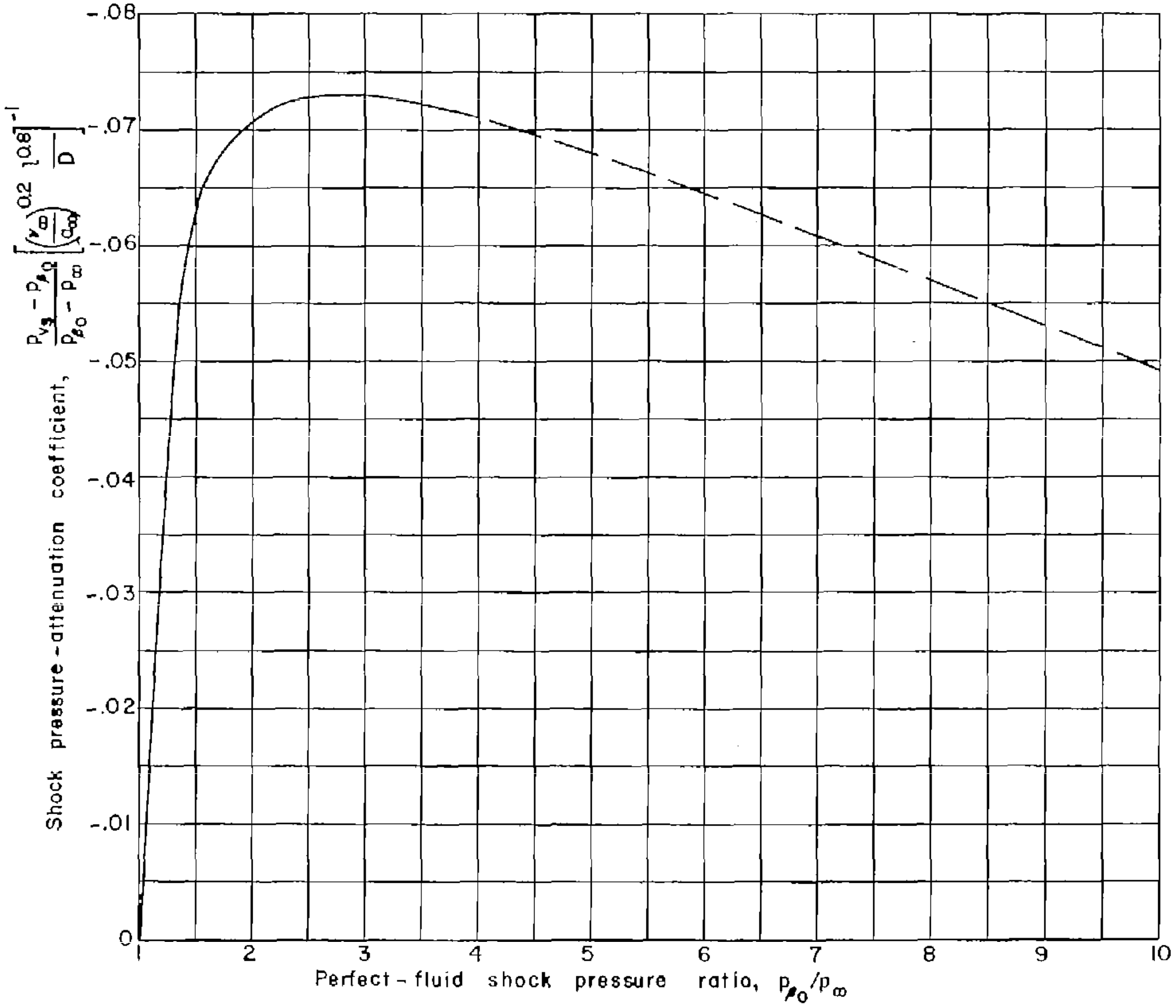

(b) Shock pressure-attenuation coefficient.

Figure 7.- Concluded.

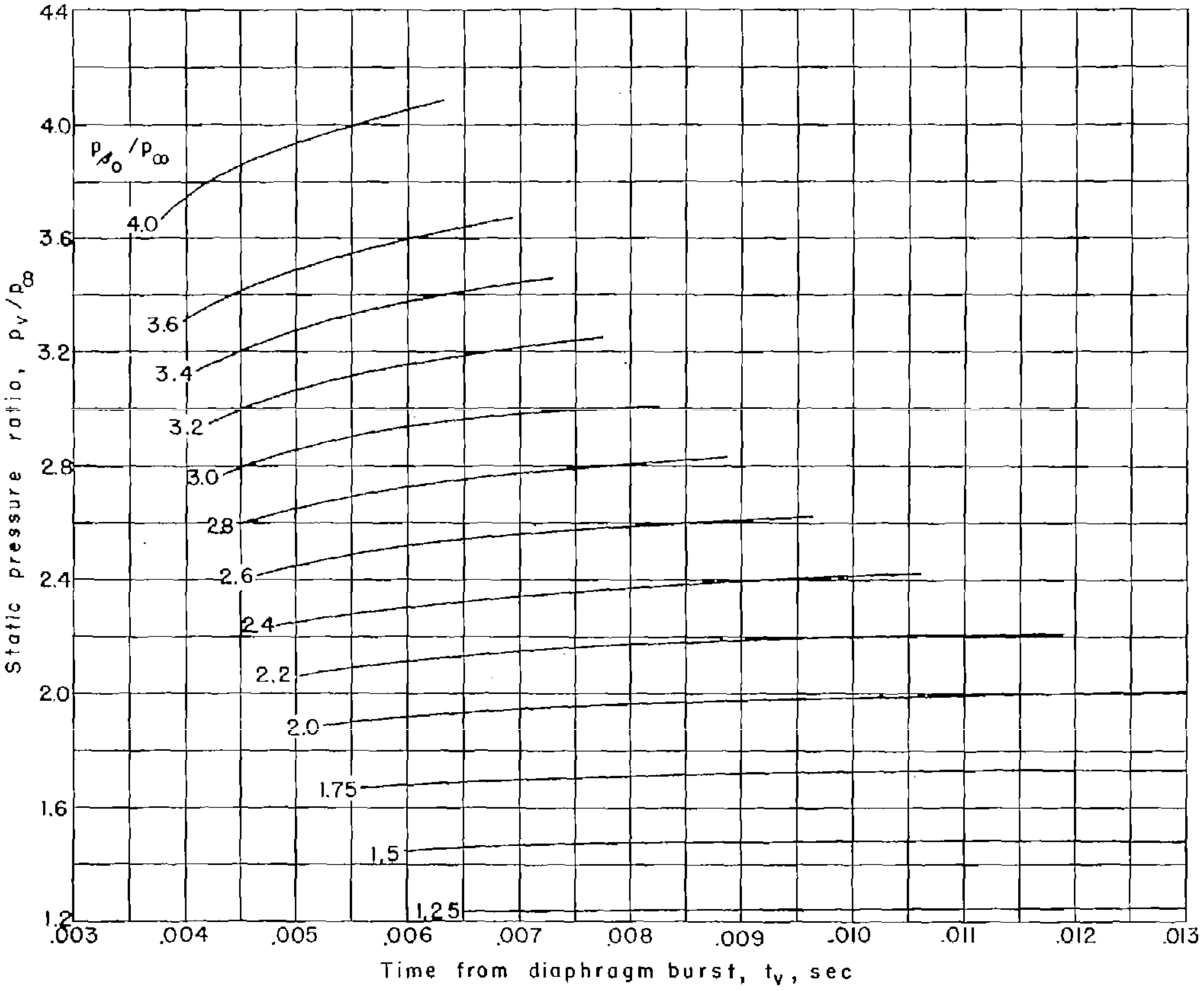

Figure 8.- Theoretical variation of static pressure ratio with time. $x = 8$ feet; $a_\epsilon = a_\infty = 1{,}117$ feet per second; $c_f = 0.0581R_e^{-1/5}$.

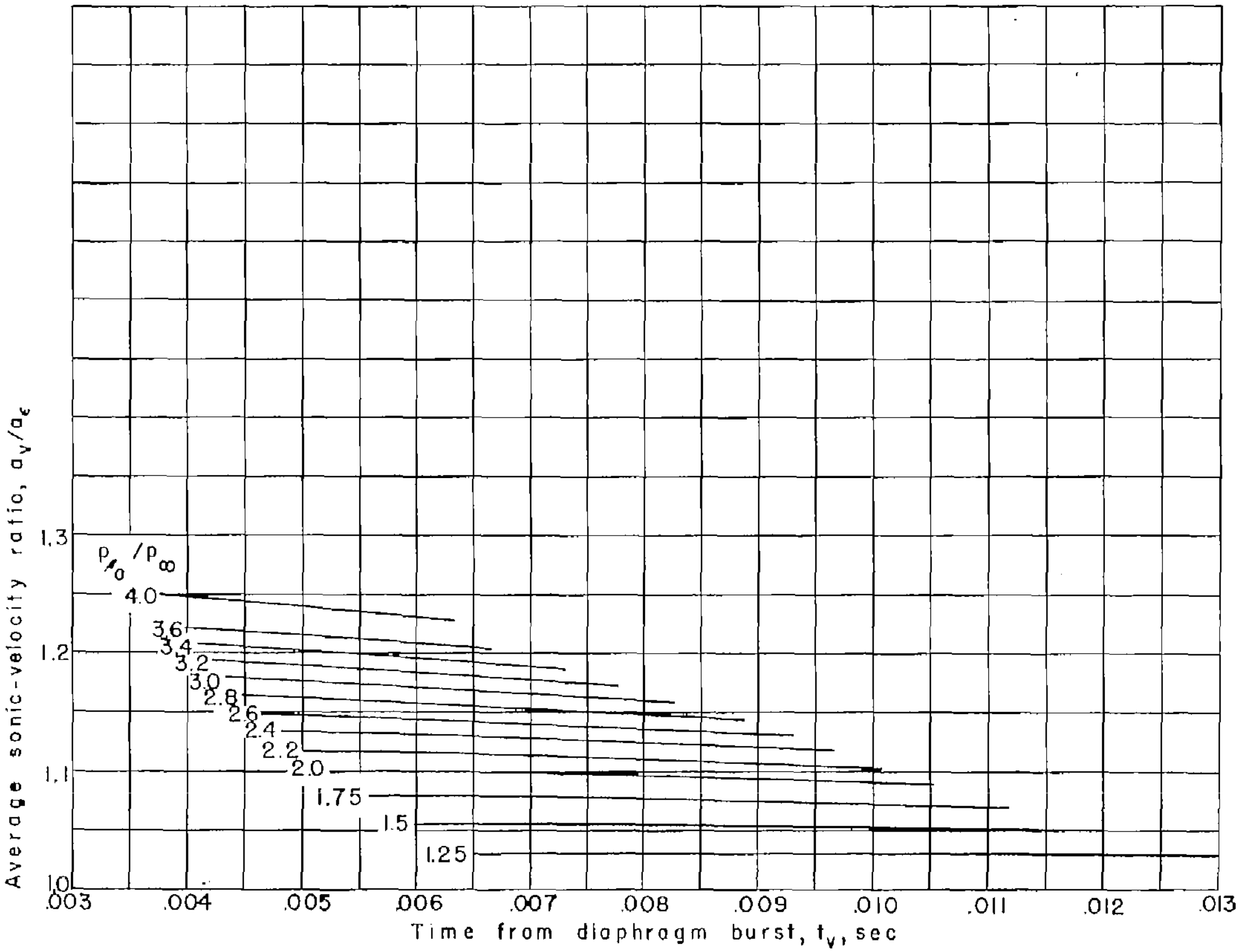

Figure 9.- Theoretical variation of average sonic-velocity ratio a_v/a_ϵ with time. $x = 8$ feet; $a_\epsilon = a_\infty = 1{,}117$ feet per second; $c_f = 0.0581R_e^{-1/5}$.

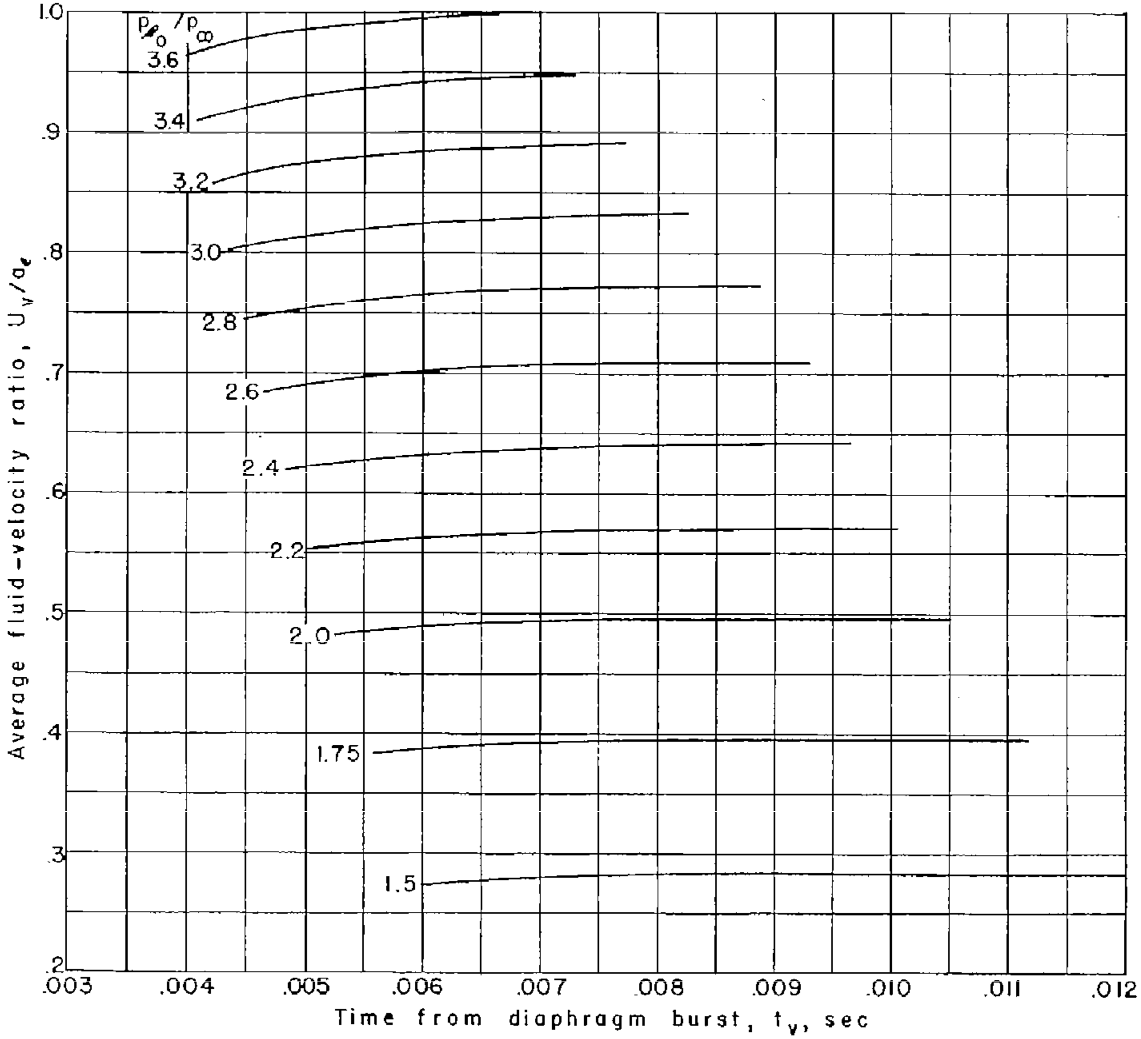

Figure 10.- Theoretical variation of average particle-velocity ratio U_v/a_ϵ with time. $x = 8$ feet; $a_\epsilon = a_\infty = 1,117$ feet per second; $c_f = 0.0581R_e^{-1/5}$.

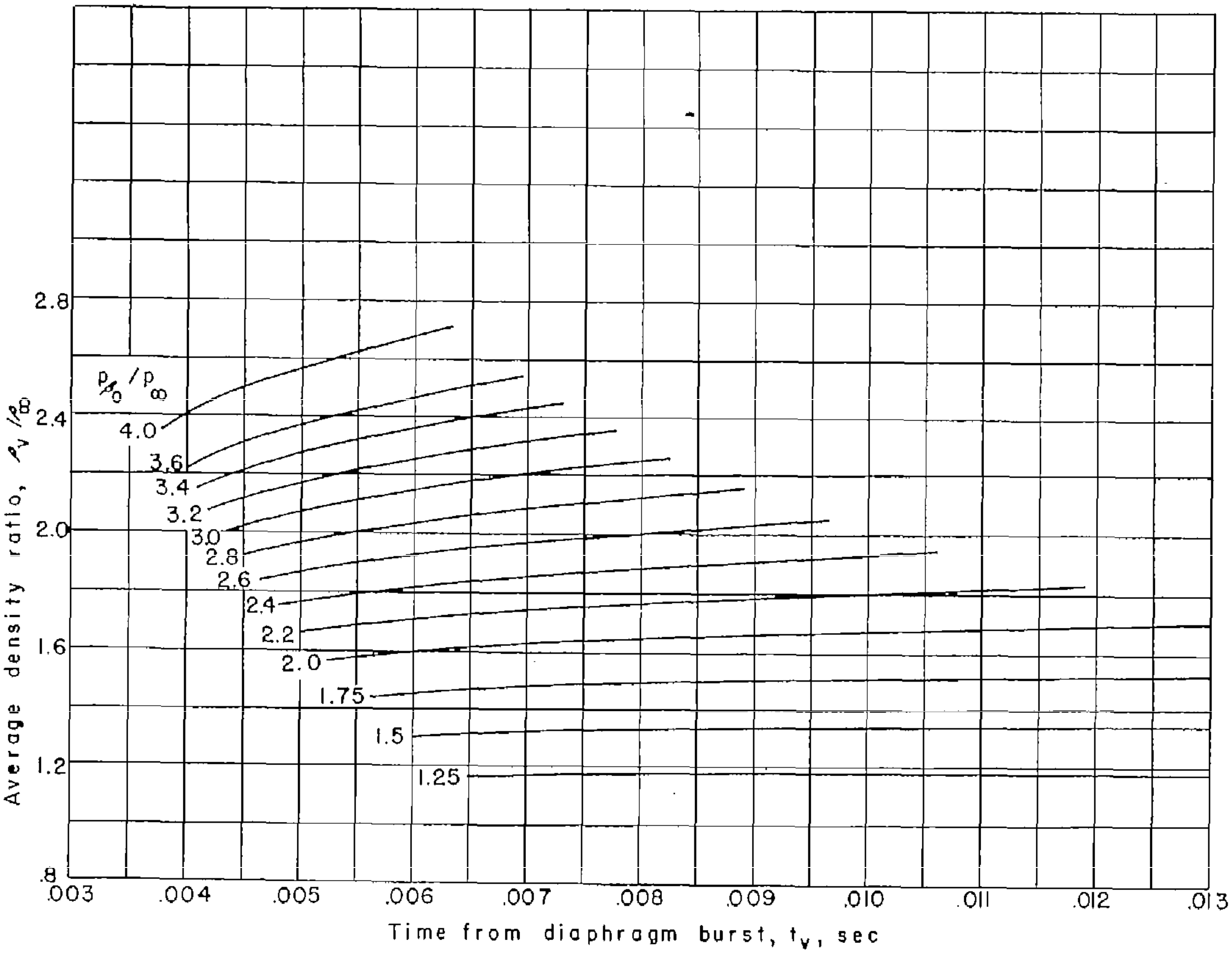

Figure 11.- Theoretical variation of average density ratio with time. $x = 8$ feet; $a_\epsilon = a_\infty = 1{,}117$ feet per second; $c_f = 0.0581R_e^{-1/5}$.

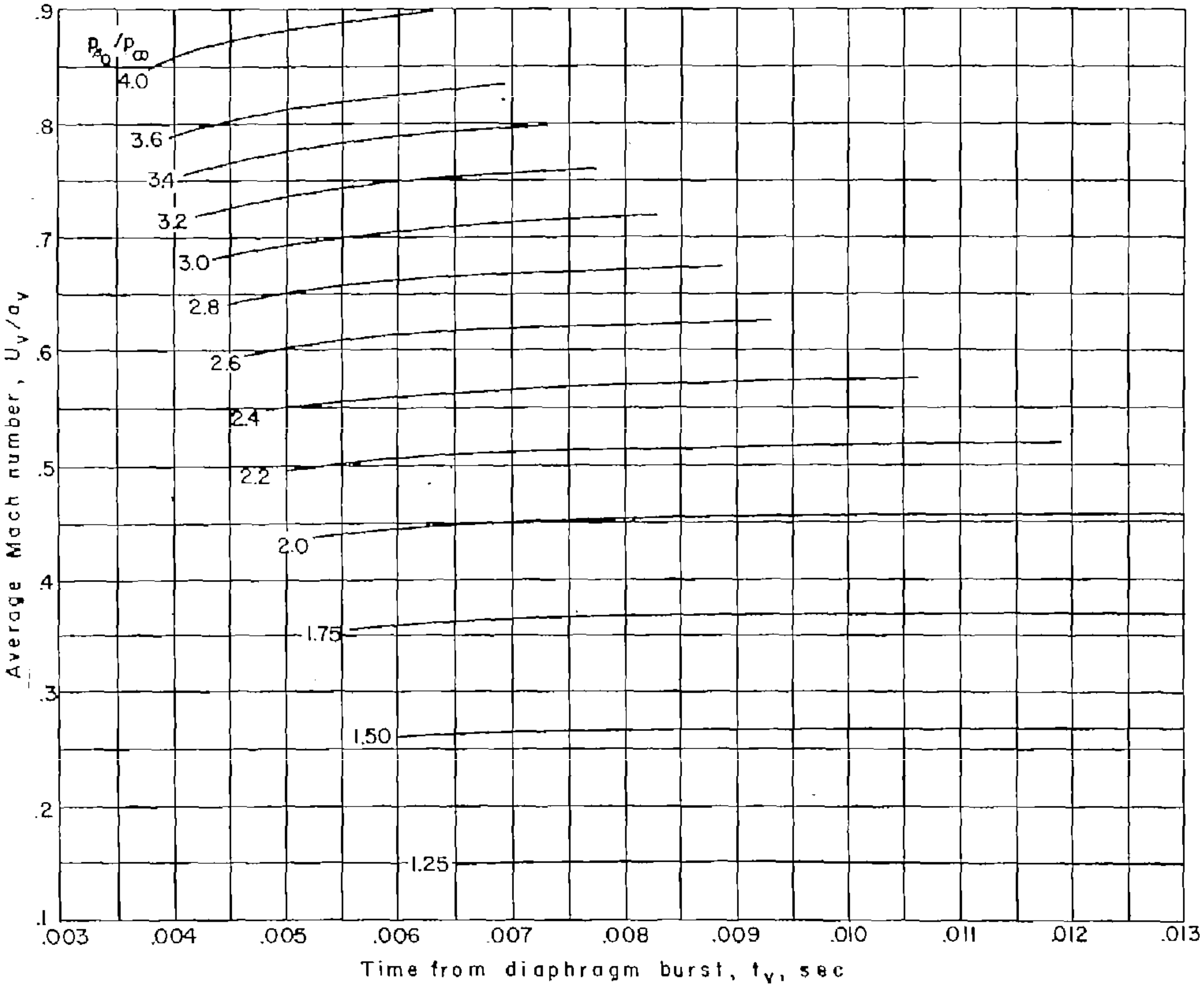

Figure 12.- Theoretical variation of average Mach number with time. $x = 8$ feet; $a_\epsilon = a_\infty = 1{,}117$ feet per second; $c_f = 0.0581 R_e^{-1/5}$.

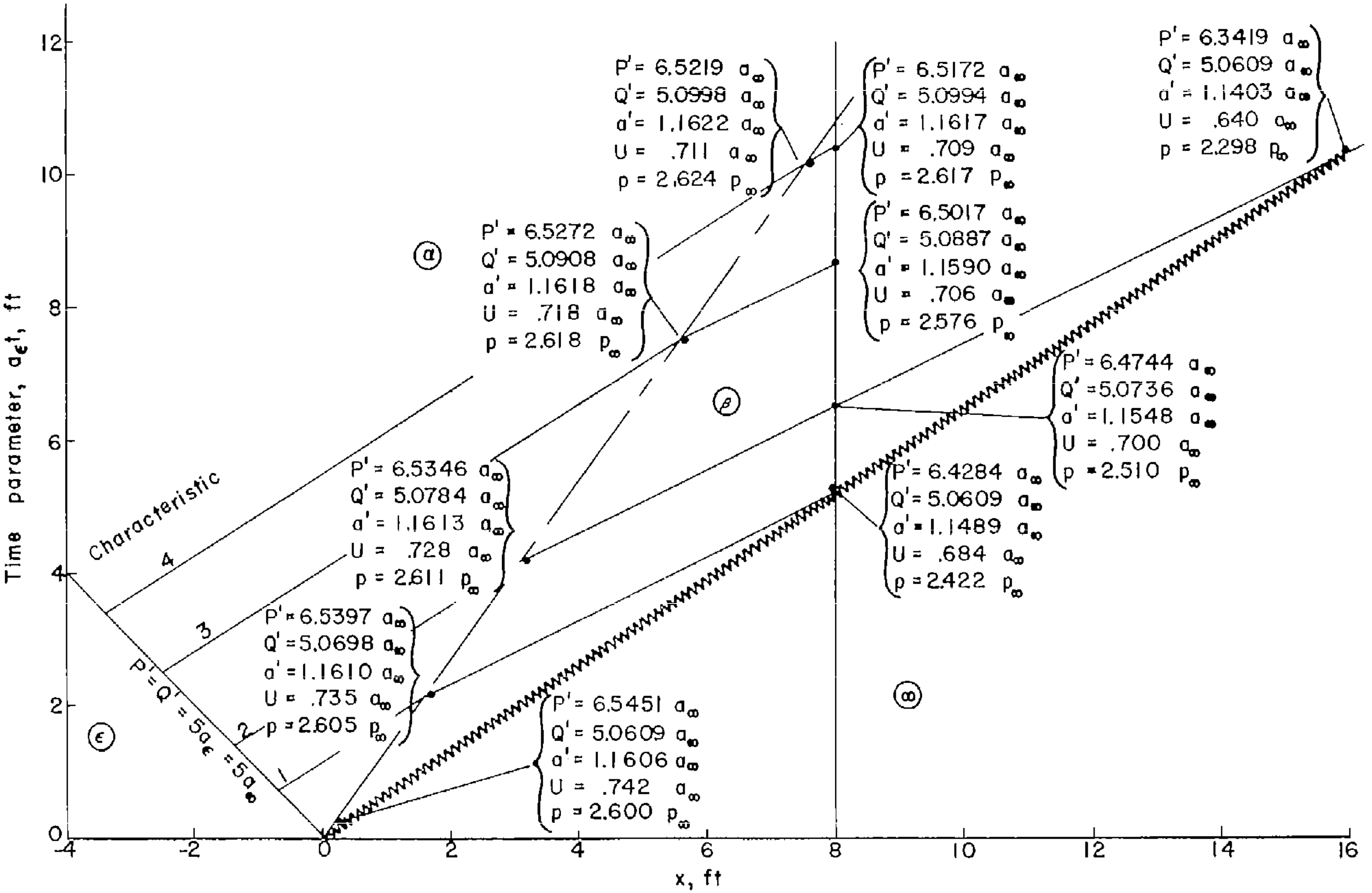

Figure 13.- Characteristic plot for shock pressure ratio of 2.60 showing generation of waves in region β.

NACA-Langley - 3-14-55 - 1000